16th International Conference on Nuclear Reaction Mechanisms

Varenna, June 12-16, 2023

CHARACTERISTICS OF THE FISSION FRAGMENTS IN THE THREE-BODY MODEL OF BINARY FISSION

Vitali Yu. DENISOV

INFN Laboratori Nazionali di Legnaro, Legnaro (Padova), Italy

Institute for Nuclear Research, Kiev, Ukraine

Department of Physics, Taras Shevchenko National University of Kiev, Ukraine

Two-body system: two heavy fragments

Interaction of two heavy nuclei

Let us consider fragments with surface radii

$$R_i(\theta) = R_{i0}\left[1 + \sum_{\ell=2}^{4} \beta_{i\ell} Y_{\ell 0}(\theta))\right],\ i = 1, 2.$$

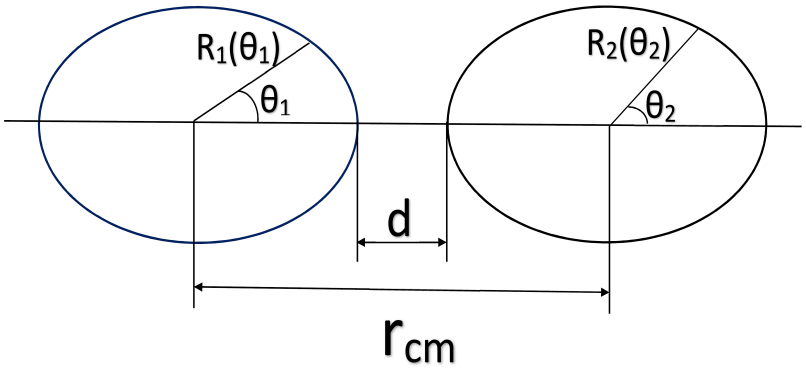

The equilibrium shape of each fragment is spherical.

The total potential energy of two deformed fission fragments after scission is

$$V_{12}^{\rm tot}(r, \beta_{1\ell}, \beta_{2\ell}) = V_{12}^{\rm Coul}(r, \beta_{1\ell}, \beta_{2\ell}) + V_{12}^{\rm nucl}(r, \beta_{1\ell}, \beta_{2\ell}) + E_{1\ \rm Liquid\ Drop}^{\rm deform}(\beta_{1\ell}) + E_{2\ \rm Liquid\ Drop}^{\rm deform}(\beta_{2\ell}).$$

Here $r = r_{\rm cm}$,

$$V_{12}^{\rm Coul}(r, \beta_{1\ell}, \beta_{2\ell}) = \frac{Z_1 Z_2 e^2}{r}[1 + f^{\rm Coul}(r, R_{10}, R_{20}, \beta_{1\ell}, \beta_{2\ell})].$$

According to the proximity theorem

$$V_{12}^{\rm nucl}(r, \beta_{1\ell}, \beta_{2\ell}) = \frac{1/R_{10}+1/R_{20}}{C_1+C_2} V_{\rm sph}^{\rm nucl}(d + R_{10} + R_{20}),$$

where C_i are the curvatures of nuclei $(i = 1, 2)$ in the closest points.

$$E_{i\ \rm Liquid\ Drop}^{\rm deform}(\beta_{i\ell}) = \frac{1}{2}\Sigma_\ell C_{i\ell}^{\rm LD} \beta_{i\ell}^2,$$

where $C_{i\ell}^{\rm LD}$ is the liquid-drop stiffness coefficient for the surface distortions of multipolarity ℓ in nucleus i.

The nuclear part of the potential between spherical nuclei consists of the macroscopic and shell-correction parts

$$V_{\rm sph}^{\rm nucl}(r) = V_{\rm macro}(r) + V_{\rm sh}(r).$$

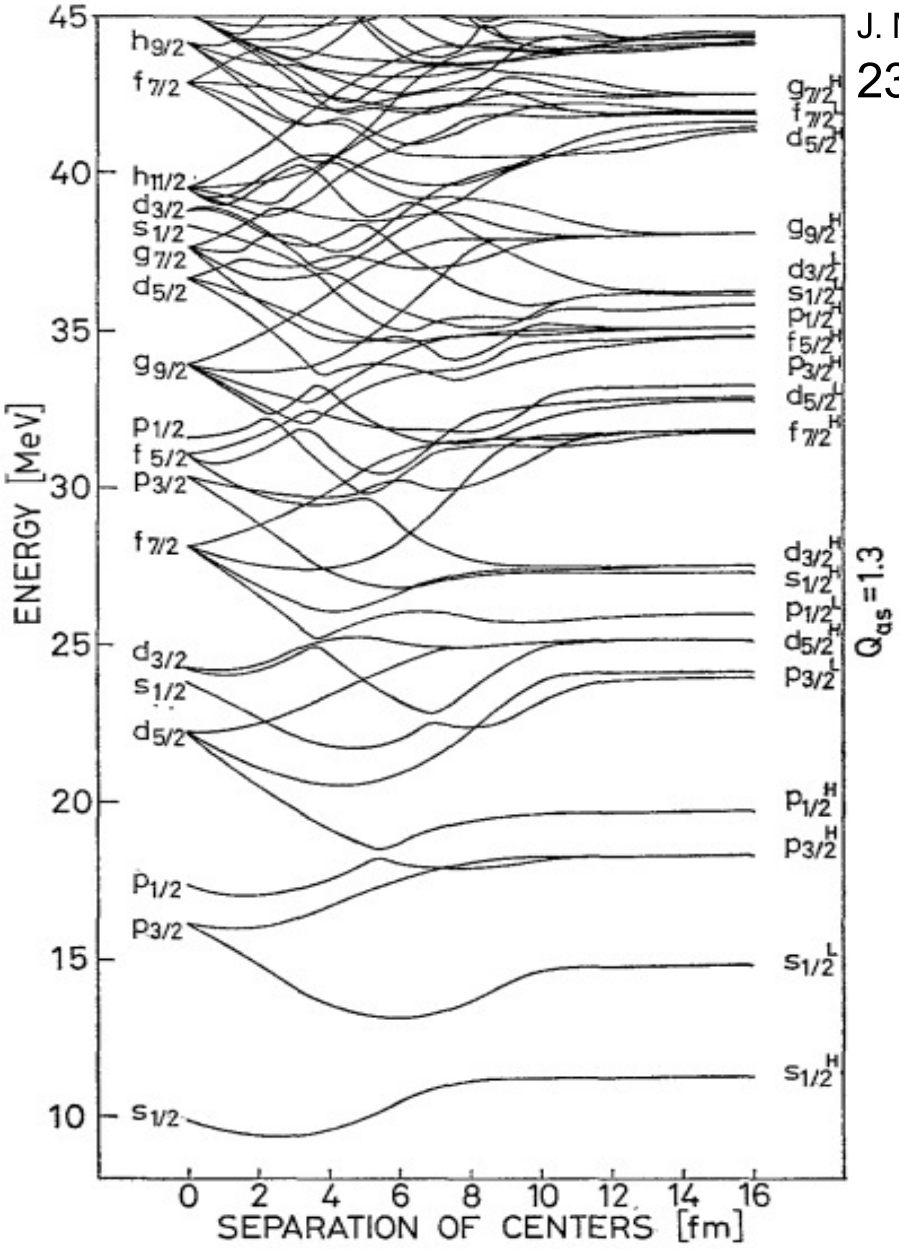

J. Maruhn, W. Greiner, Z. Phys. 251, 431 (1972).

238 => 164 + 74

Shell correction method:

$E=E_{macro}+E_{shell}$

$E_{shell}=\Sigma_i\ \varepsilon_i - \langle\Sigma_i\ \varepsilon_i\rangle$

36Ar=>16O+20Ne

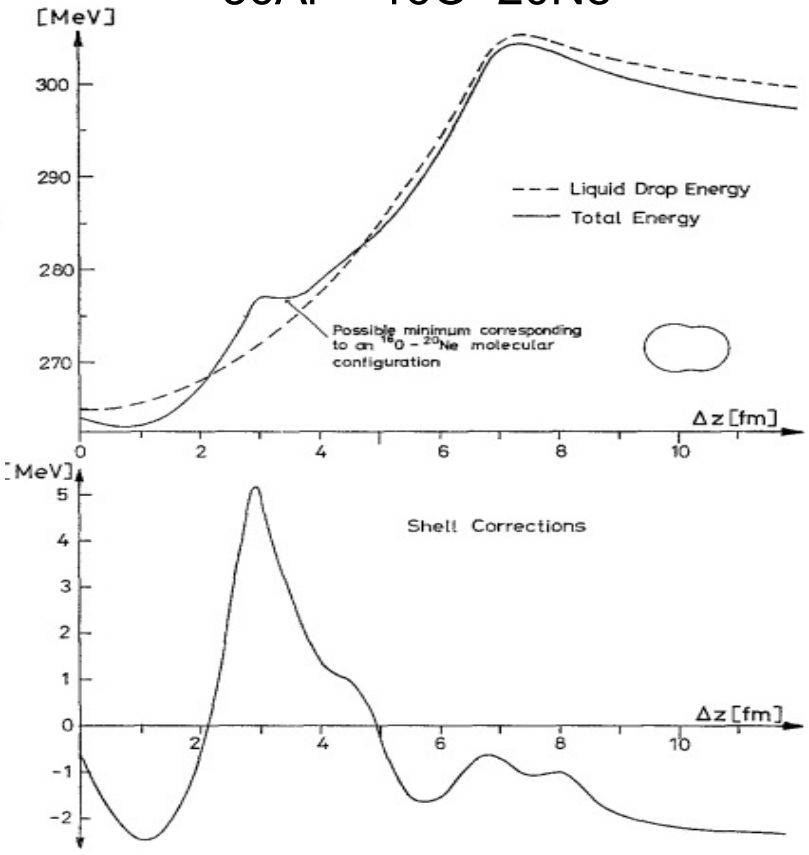

$$V_{\rm sph}^{\rm nucl}(r) = V_{\rm macro}(r) + V_{\rm sh}(r).$$

The macroscopic part at $r > R_{0\rm t}$:

$$V_{\rm macro}(r) = \left[v_1 c + v_2 c^{1/2}\right] / \left\{1 + \exp\left[\frac{r - R_{0\rm t}}{d_1 + d_2/c}\right]\right\},$$

where v_1, v_2, d_1, d_2 are constants,

$c = R_{01}R_{02}/R_{0\rm t}$, $R_{0\rm t} = R_{10} + R_{20}$, and R_{0k} is the radius of nucleus k.

The shell-correction part:

$$V_{\rm sh}(r) = [\delta E_1 + \delta E_2]\left\{1/\left[1 + \exp\left(\frac{R_{\rm sh} - R}{d_{\rm sh}}\right)\right] - 1\right\},$$

where $\delta E_k = B_k^{\rm macro}(A_k, Z_k) - B_k^{\rm exp}(A_k, Z_k)$ is the phenomenological shell correction for nucleus k, $B_k^{\rm macro}$ is the macroscopic binding energy calculated by the formula, $B_k^{\rm exp}(A, Z)$ is the experimental binding energy, $R_{\rm sh} = R_{0\rm t} - 0.26$ fm, and $d_{\rm sh} = 0.233$ fm.

The potential parameters are found by fitting the empirical barrier heights of the 89 nucleus-nucleus systems as well as semi-microscopic potentials calculated for 1485 nucleus-nucleus systems at 12 distances around touching points.

The differences between 89 empirical barrier heights and barrier heights evaluated using the potential with the shell correction contribution (relax), frozen-density (frozen), Krappe-Nix-Sierk (KNS), Bass (Bass80), Bass (Bass74), proximity (Prox77), proximity (Prox2000), Akyuz-Winter, and Siwek-Wilczynska-Wilczynski (SWW) potentials.

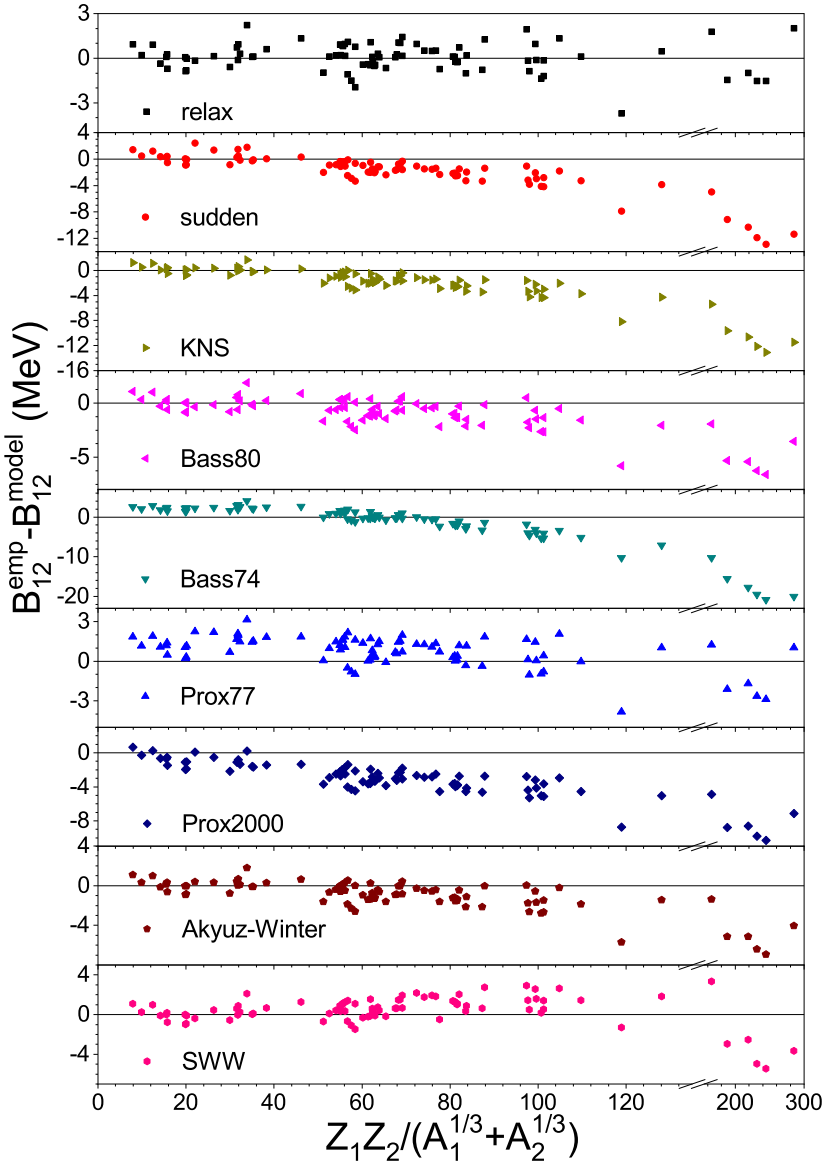

$V_{12}^{\rm tot}(r,\beta_{1\ell},\beta_{2\ell}) = V_{12}^{\rm Coul}(r,\beta_{1\ell},\beta_{2\ell}) + V_{12}^{\rm nucl}(r,\beta_{1\ell},\beta_{2\ell}) + E_{1\ {\rm Liquid\ Drop}}^{\rm deform}(\beta_{1\ell}) + E_{2\ {\rm Liquid\ Drop}}^{\rm deform}(\beta_{2\ell}).$

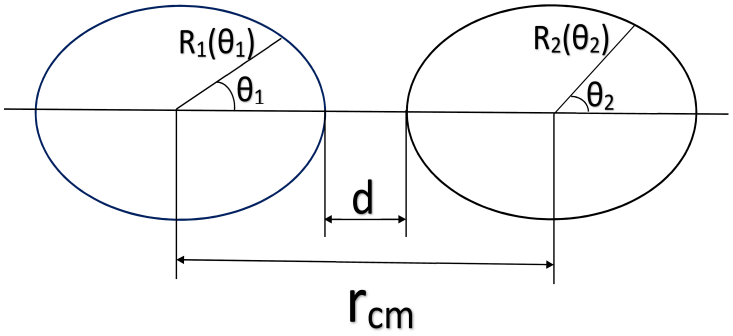

$R_i(\theta) = R_{i0}\left[1 + \sum_{\ell=2}^{4} \beta_{i\ell} Y_{\ell 0}(\theta))\right],\ i = 1, 2.$

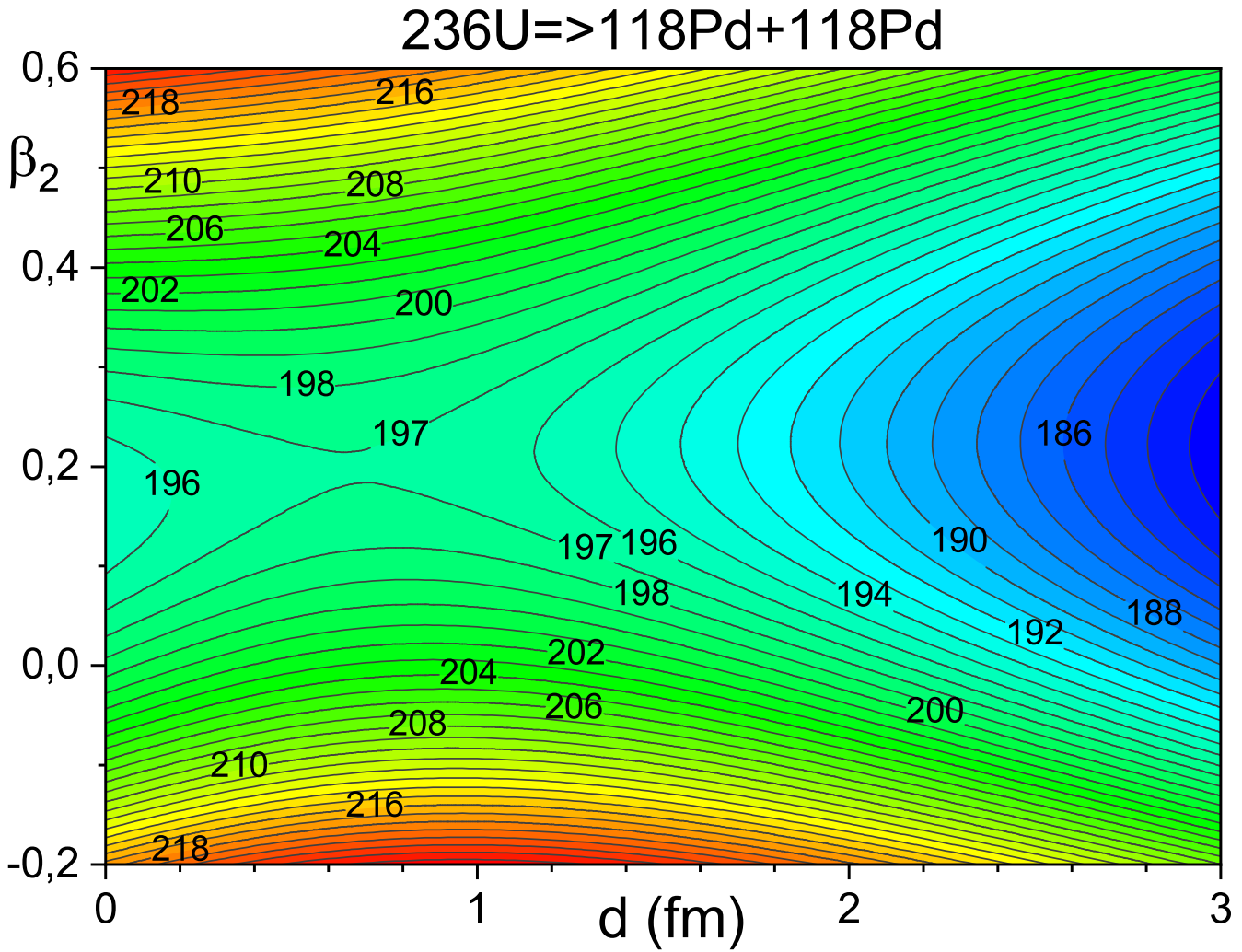

The total potential $V_{12}^{\rm tot}(r,\beta_2)$ is found using the minimization of $V_{12}^{\rm tot}(r,\beta_{12},\beta_{22},\beta_{13},\beta_{23},\beta_{14},\beta_{24})$ on β_{i3} and β_{i4} for each point (d,β_2). Here $\beta_{12} = \beta_{22} = \beta_2$.

The Q-value $Q = 2 \times BE(^{118}{\rm Pd}) - BE(^{236}{\rm U}) = 2 \times 991.816 - 1790.411 = 193.221$ MeV.

$Q \approx 193$ MeV $< V_{12\ {\rm saddle\ point}}^{\rm tot} \approx 197$ MeV.

Three-body system: two heavy fragments and α-particle between them

Ternary fission is the proof of the existence of the three-body scission shape with $\alpha-$particle.

Three-body system: two heavy fragments and α-particle between them

Ternary fission is the proof of the existence of the three-body scission shape with $\alpha-$particle.

The microscopic models confirm the formation of $\alpha-$particle or clusters of density at scission.

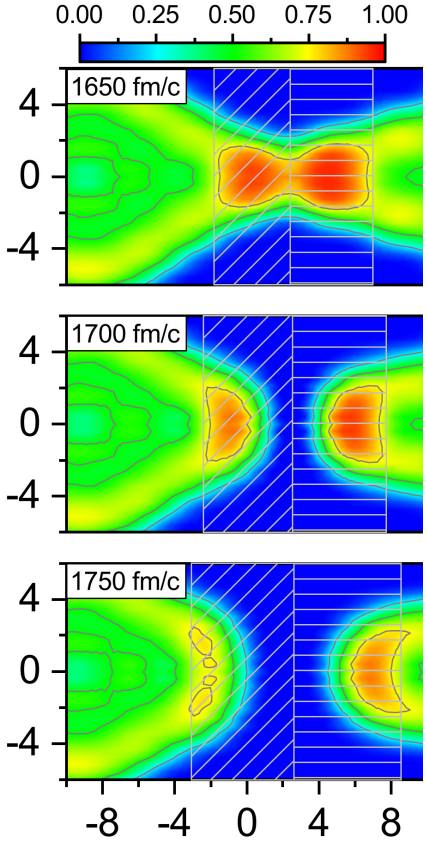

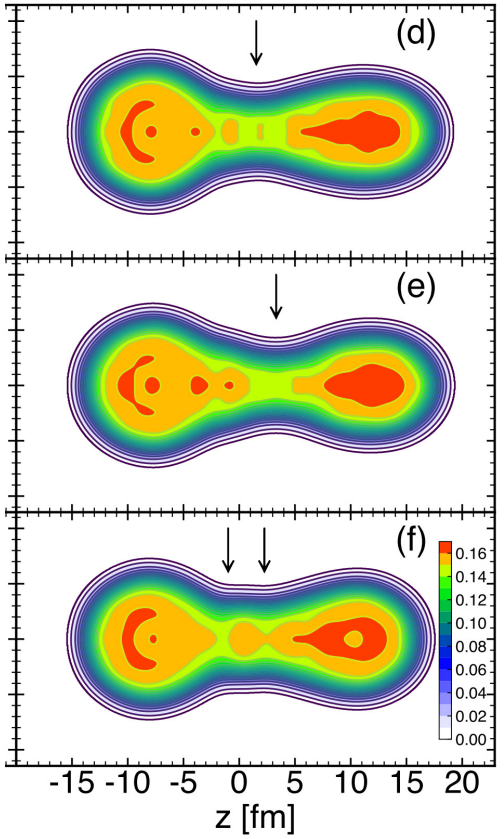

The proton localization along the fission trajectory in the time-dependent density functional model. Z.X. Ren, D. Vretenar, T. Niksic, P.W. Zhao, J. Zhao, J. Meng, Dynamical Synthesis of ^{4}He in the Scission Phase of Nuclear Fission, Phys. Rev. Lett. 128, 172501 (2022) [Supplemental Material].

Nuclear density distributions near the scission point calculated in the framework of the Hartree-Fock-Bogoliubov approximation. R. Han, M. Warda, A. Zdeb, L. M. Robledo, Phys. Rev. C 104, 064602 (2021). The smallest radius of the neck is $\simeq 2$ fm. The radius of the alpha-particle is 2.13 fm.

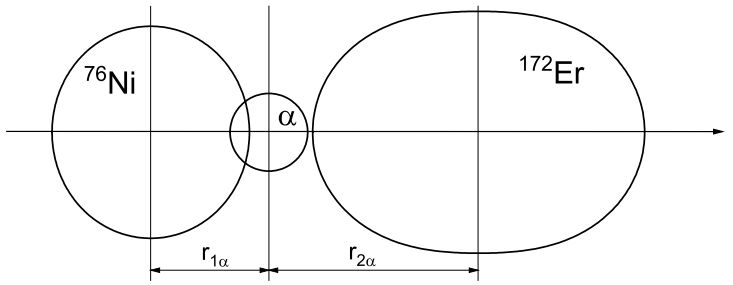

Let us consider the systems ^{76}Ni$(\beta_1 = -0.074) + \alpha +^{172}$ Er$(\beta_2 = 0.351)$:

The total potential energy of two heavy fission fragments and α-particle between them is

$$V^{\rm tot}_{1\alpha 2}(r_{1\alpha}, r_{2\alpha}, \beta_{12}, \beta_{22}) = V^{\rm tot}_{12}(r_{1\alpha} + r_{2\alpha}, \beta_{12}, \beta_{22}) + V^{\rm Coul}_{1\alpha}(r_{1\alpha}, \beta_{12}) + V^{\rm nucl}_{1\alpha}(r_{1\alpha}, \beta_{12}) + V^{\rm Coul}_{2\alpha}(r_{2\alpha}, \beta_{22}) + V^{\rm nucl}_{2\alpha}(r_{2\alpha}, \beta_{22}).$$

The nuclear part of the **α-nucleus potential** of the Woods-Saxon shape are obtained using the data for the ground-state-to-ground-state α-transition half-lives in 401 nuclei and the α-capture cross-sections of ^{40}Ca, ^{44}Ca, ^{59}Co, ^{208}Pb, and ^{209}Bi (**U**nified **M**odel for **A**lpha-**D**ecay and **A**lpha-**C**apture).

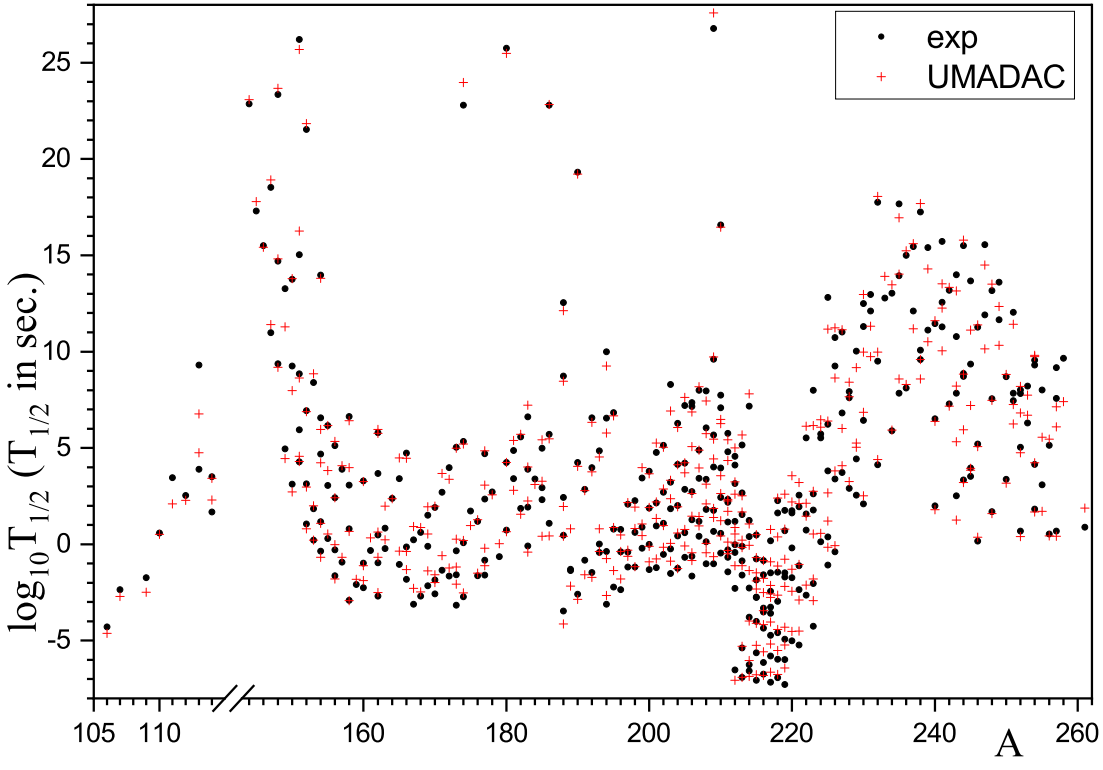

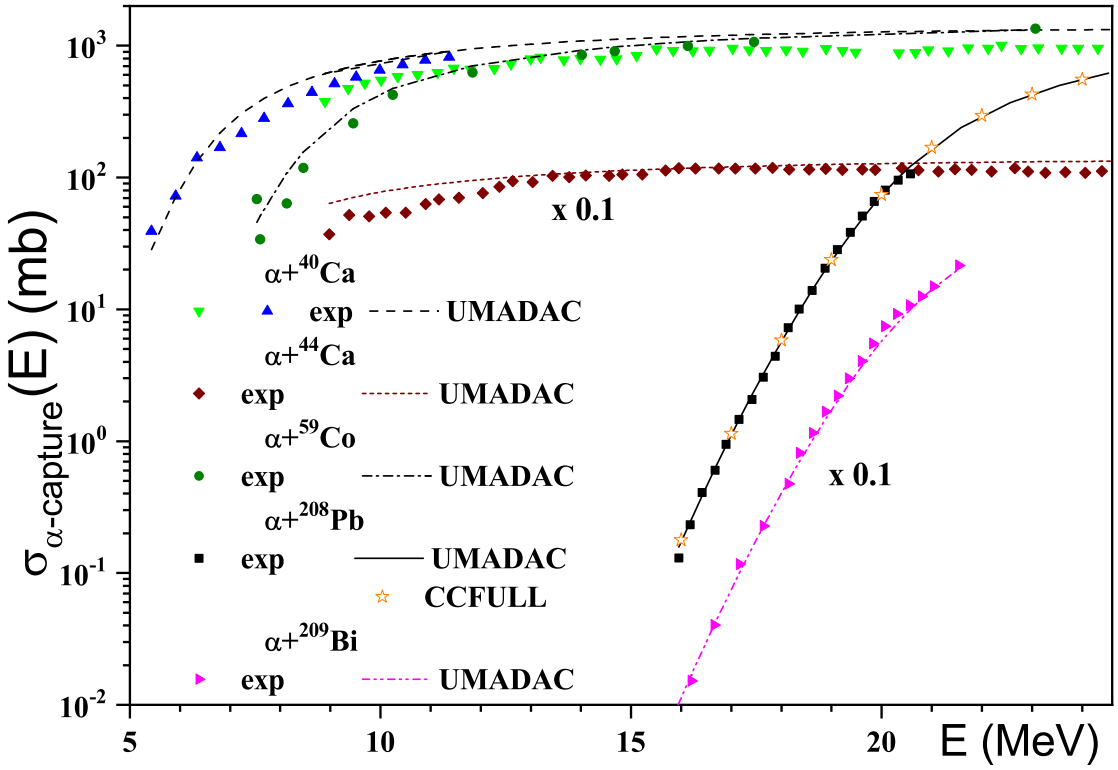

$$V^{\rm tot}_{1\alpha 2}(r_{1\alpha}, r_{2\alpha}, \beta_{12}, \beta_{22}) = V^{\rm tot}_{12}(r_{1\alpha} + r_{2\alpha}, \beta_{12}, \beta_{22}) + V^{\rm Coul}_{1\alpha}(r_{1\alpha}, \beta_{12}) + V^{\rm nucl}_{1\alpha}(r_{1\alpha}, \beta_{12}) + V^{\rm Coul}_{2\alpha}(r_{2\alpha}, \beta_{22}) + V^{\rm nucl}_{2\alpha}(r_{2\alpha}, \beta_{22}).$$

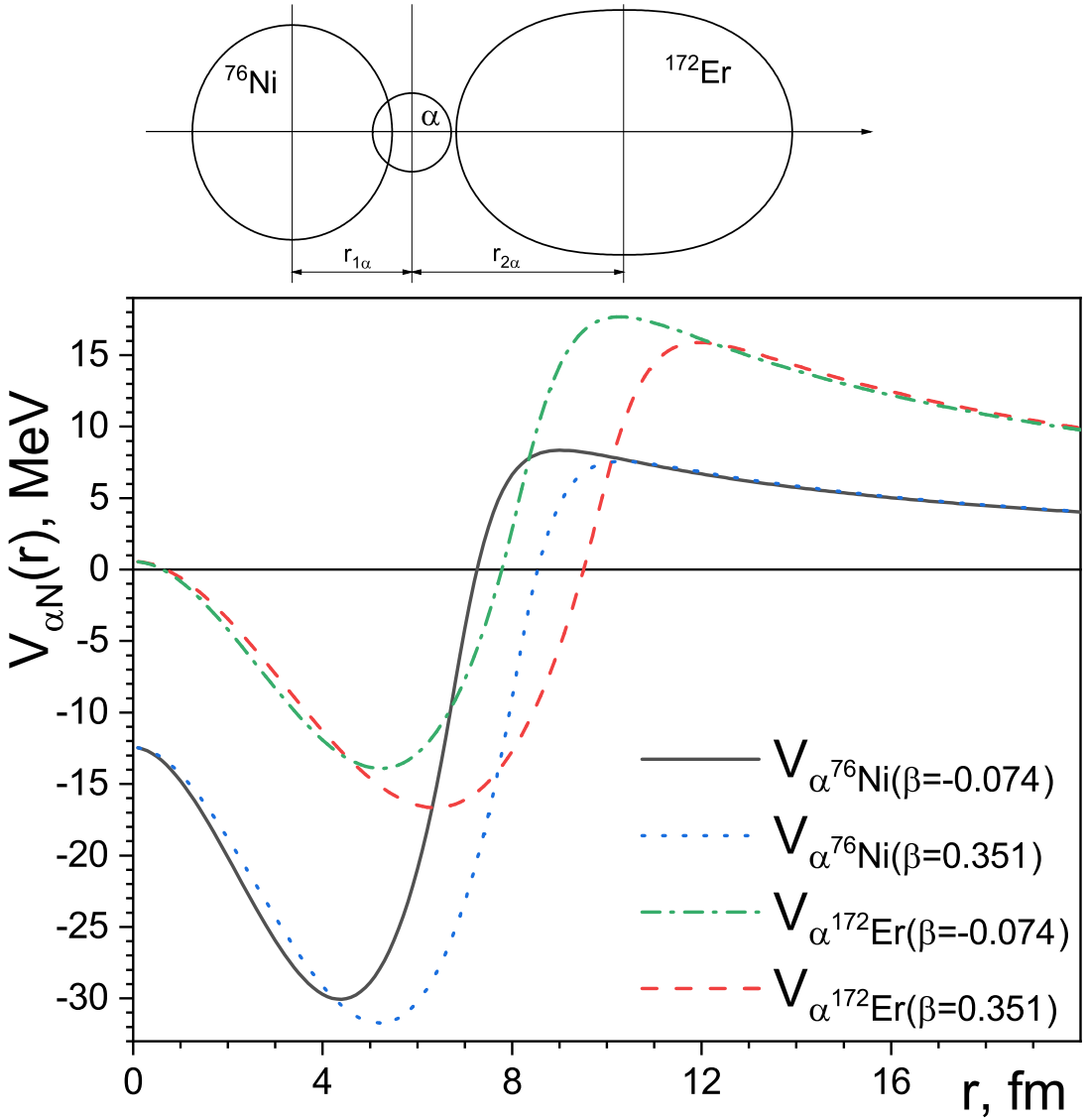

The radial dependencies of potentials for the systems α+^{76}Ni and α+^{172}Er.

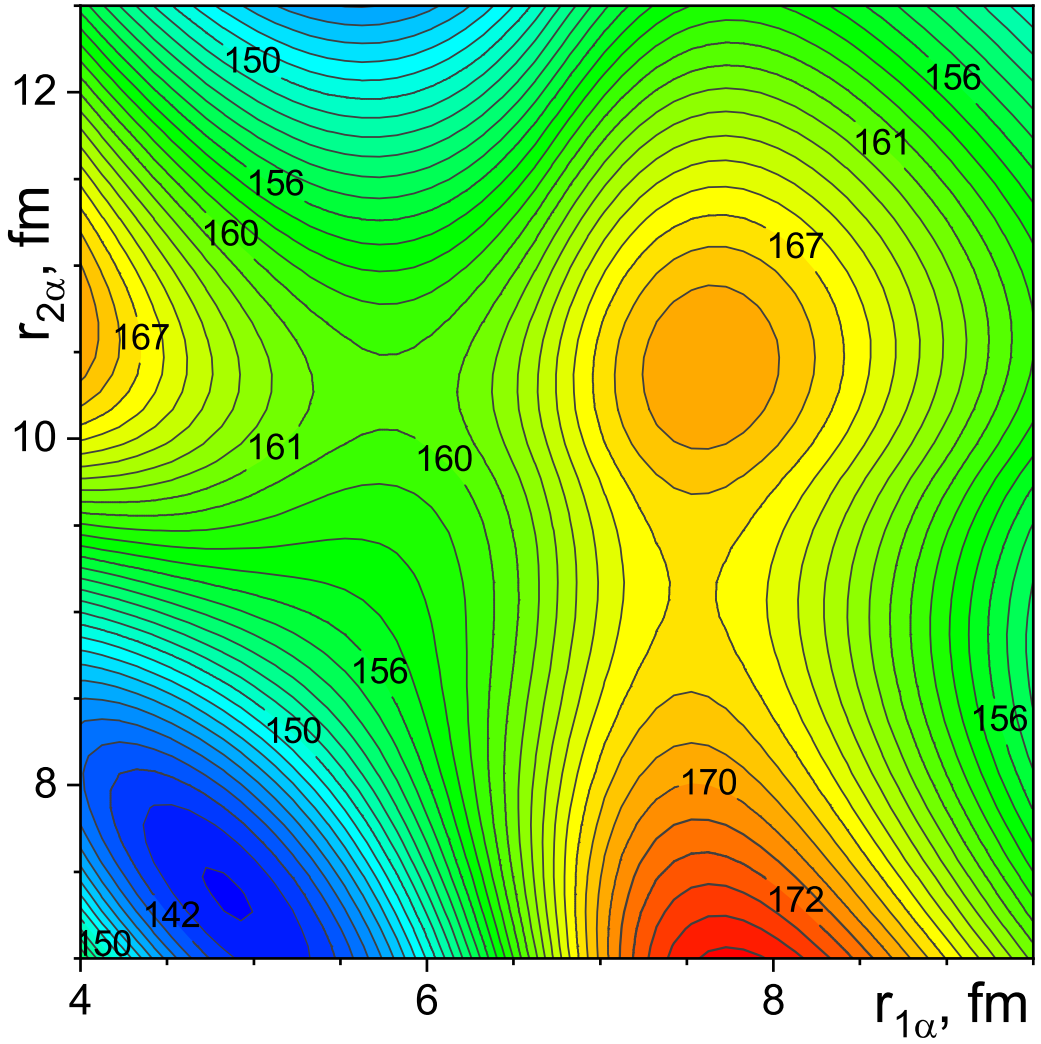

The total interaction potential energy $V^{\rm total}_{1\alpha 2}(r_{1\alpha}, r_{2\alpha}, \beta_1, \beta_2)$ for the system $^{76}{\rm Ni}(\beta_1 = -0.074) + \alpha + ^{172}{\rm Er}(\beta_2 = 0.351)$.

$r^{\rm barrier}_{\alpha^{76}{\rm Ni}} \approx 8$ fm $> r^{\rm saddle\ point}_{1\alpha} \approx 6$ fm, therefore, α-particle fuses with ^{76}Ni at $r_{2\alpha} > 11$ fm.

Therefore, it leads to the binary fission.

The yield of the primary fission fragments

The yield of the primary fission fragments with the nucleon compositions $[A_1, Z_1]$ and $[A_2 = A_{\rm cn} - A_1, Z_2 = Z_{\rm cn} - Z_1]$ formed through the first and second saddle points of the three-body scission configuration is

$$Y_3(A_1, Z_1) = \frac{2\left[\rho_{12}^{\text{saddle }1}(A_1, Z_1) + \rho_{12}^{\text{saddle }2}(A_1, Z_1)\right]}{N_3},$$

where

$$\rho_{12}^{\text{saddle }1}(A_1, Z_1) = \int d\beta_1 \int d\beta_2 \rho_{A_1-4, Z_1-2}(E_1^{s1}) \rho_{A_2, Z_2}(E_2^{s1}), \rho_{12}^{\text{saddle }2}(A_1, Z_1) = \int d\beta_1 \int d\beta_2 \rho_{A_1, Z_1}(E_1^{s2}) \rho_{A_2-4, Z_2-2}(E_2^{s2})$$

are the energy level density of the three-fragment system above the saddle point barrier 1 and 2 respectively,

$$N_3 = \sum_{A_1, Z_1} \left[\rho_{12}^{\text{saddle }1}(A_1, Z_1) + \rho_{12}^{\text{saddle }2}(A_1, Z_1)\right]$$

is the sum on all possible values A_1 and Z_1, β_k is the quadrupole deformation parameter of the surface.

$$\rho_{A,Z}(U) = \frac{\sqrt{\pi}}{12(a_{\rm dens} U^5)^{1/4}} \exp\left[2\sqrt{a_{\rm dens} U}\right].$$

is the back-shifted Fermi gas energy level density, $U = E - \delta$,

$$a_{\rm dens} = a_{\rm inf}\left[1 + \frac{\delta_{\rm shell}}{U}(1 - \exp\left(-\gamma U\right))\right].$$

E_1^{s1}, E_2^{s1}, E_1^{s2}, and E_2^{s2} are the thermal excitation energies of the nascent fragments. α-particle is the inert particle.

$$\frac{E_1^{s1} - \delta_1^{s1}}{a_{\rm dens}(A_1, E_1^{s1})} \equiv (T_1^{s1})^2 = (T_2^{s1})^2 \equiv \frac{E_2^{s1} - \delta_2^{s1}}{a_{\rm dens}(A_2, E_2^{s1})}, \quad E_1^{s1} + E_2^{s1} = Q_3^{s1} + E_{\rm cn} - B_{1\alpha 2}^{s1}(r_{\beta_1,\beta_2});$$

$$\frac{E_1^{s2} - \delta_1^{s2}}{a_{\rm dens}(A_1, E_1^{s2})} \equiv (T_1^{s2})^2 = (T_2^{s2})^2 \equiv \frac{E_2^{s2} - \delta_2^{s2}}{a_{\rm dens}(A_2, E_2^{s2})}, \quad E_1^{s2} + E_2^{s2} = Q_3^{s2} + E_{\rm cn} - B_{1\alpha 2}^{s2}(r_{\beta_1,\beta_2}).$$

The temperatures of the fragments are the same ($T_1^{s_k} = T_2^{s_k}$) in each saddle-point.

Steps for the calculation of the yields of elements

1. Calculation of the fission Q-values, which lead to the same final fission fragments $[A_{\rm cn}, Z_{\rm cn}] \Rightarrow [A_1, Z_1] + [A_{\rm cn} - A_1, Z_{\rm cn} - Z_1]$ by passing through the different saddle points ($Q_3^{s1} = B_{\rm exp}(A_1 - 4, Z_1 - 2) + B_{\rm exp}(A_2, Z_2) + B_{\rm exp}(4, 2) - B_{\rm exp}(A_{\rm cn}, Z_{\rm cn})$, $Q_3^{s2} = B_{\rm exp}(A_1, Z_1) + B_{\rm exp}(A_2 - 4, Z_2 - 2) + B_{\rm exp}(4, 2) - B_{\rm exp}(A_{\rm cn}, Z_{\rm cn})$). Here $B_{\rm exp}(A, Z)$ is the experimental binding energy of the nucleus with A nucleons and Z protons.

2. Calculation of the saddle point heights $B_{1\alpha 2}^{s1}(r_{\beta_1,\beta_2})$ and $B_{1\alpha 2}^{s2}(r_{\beta_1,\beta_2})$ for the pointed fragment partitions at given values of the fragment deformations β_i.

3. Calculation of the excitation energy of each fragment E_k^{si} by equating the temperatures of fragments in dependence on the chosen saddle point.

4. Calculation of the product of the levels density of the system $\rho_{A_1,Z_1}(E_1^{si})\rho_{A_2,Z_2}(E_2^{si})$ presented in the integrals for evaluation $\rho_{12}^{\rm saddle\ i}(A_1, Z_1)$ using the fragment excitation energies E_k^{si}.

5. Calculation of $\rho_{12}^{\rm saddle\ i}(A_1, Z_1)$ by taking the integral for all possible values of β_i.

6. Repeat steps 1-5 for all possible fission fragment variants $[A_1, Z_1]$ and $[A_{\rm cn} - A_1, Z_{\rm cn} - Z_1]$.

7. Calculation of the norm $N_3 = \sum_{A_1,Z_1} \left[\rho_{12}^{\rm saddle\ 1}(A_1, Z_1) + \rho_{12}^{\rm saddle\ 2}(A_1, Z_1)\right]$.

8. Calculation of the nuclide yield: $Y_3(A_1, Z_1) = 2\left[\rho_{12}^{\rm saddle\ 1}(A_1, Z_1) + \rho_{12}^{\rm saddle\ 2}(A_1, Z_1)\right]/N_3$. The mass and charge distributions of fission fragments are found using $Y(A) = \Sigma_Z Y(A, Z)$ and $Y(Z) = \Sigma_A Y(A, Z)$, respectively.

Experimental data

The experimental data for 26461 the yields $[Y_{\rm exp}(A,Z)]$ of fission fragments formed in the neutron capture reactions by ^{227,229,232}Th, ^{231}Pa, ^{237,238}Np, ^{232,233,234,235,236,237,238}U, ^{238,239,240,241,242}Pu, ^{241,243}Am, ^{242,243,244,245,246,248}Cm, ^{249,251}Cf, ^{254}Es, and ^{255}Fm are given in JENDL. The values of $Y_{\rm exp}(A,Z)$ belong to the range $10^{-21} \lesssim Y_{\rm exp}(A,Z) \lesssim 10^{-1}$.

Selection rule for the data points:

1. $Y_{\rm exp.}(A,Z) \geq 10^{-8}$.
2. $Y_{\rm exp.}(A,Z) \geq 10^{-3} Y_{\rm exp.}(A) = 10^{-3} \sum_Z Y_{\rm exp.}(A,Z)$ and $Y_{\rm exp.}(A_2 = A_{\rm cn} - A, Z_2 = Z_{\rm cn} - Z) \geq 10^{-8}$.

As a result, 9020 experimental values of $Y_{\rm exp.}(A,Z)$ are selected.

Experimental data

The experimental data for 26461 the yields $[Y_{\rm exp}(A,Z)]$ of fission fragments formed in the neutron capture reactions ^{227,229,232}Th, ^{231}Pa, ^{237,238}Np, ^{232,233,234,235,236,237,238}U, ^{238,239,240,241,242}Pu, ^{241,243}Am, ^{242,243,244,245,246,248}Cm, ^{249,251}Cf, ^{254}Es, and ^{255}Fm are given in JENDL. The values of $Y_{\rm exp}(A,Z)$ belong to the range $10^{-21} \lesssim Y_{\rm exp}(A,Z) \lesssim 10^{-1}$.

Selection rule for the data points:

1. $Y_{\rm exp.}(A,Z) \geq 10^{-8}$.
2. $Y_{\rm exp.}(A,Z) \geq 10^{-3} Y_{\rm exp.}(A) = 10^{-3} \sum_Z Y_{\rm exp.}(A,Z)$ and $Y_{\rm exp.}(A_2 = A_{\rm cn} - A, Z_2 = Z_{\rm cn} - Z) \geq 10^{-8}$.

As a result, 9020 experimental values of $Y_{\rm exp.}(A,Z)$ are selected.

The root mean square deviation

$$\delta = \sqrt{\sum_{A,Z} \left\{ \log_{10}\left[Y_{\rm theor.}(A,Z)\right] - \log_{10}\left[Y_{\rm exp.}(A,Z)\right] \right\}^2 / N}.$$

Nucl.	N	δ	Nucl.	N	δ	Nucl.	N	δ	Nucl.	N	δ	Nucl.	N	δ
^{228}Th	283	0.8435	^{230}Th	259	1.1092	^{233}Th	310	1.2287	^{232}Pa	318	0.7965	^{233}U	328	1.1215
^{234}U	315	0.7210	^{235}U	294	0.7035	^{236}U	305	0.8289	^{237}U	216	0.9596	^{238}U	289	0.7845
^{239}U	328	0.8605	^{238}Np	312	0.7211	^{239}Np	298	0.6675	^{239}Pu	338	0.6580	^{240}Pu	305	0.7999
^{241}Pu	302	0.7391	^{242}Pu	295	0.8458	^{243}Pu	292	0.7990	^{242}Am	310	0.7742	^{244}Am	286	0.9742
^{243}Cm	306	0.9757	^{244}Cm	337	0.7311	^{245}Cm	302	0.9726	^{246}Cm	311	0.7676	^{247}Cm	300	0.8311
^{249}Cm	294	0.9573	^{250}Cf	337	0.9903	^{252}Cf	287	0.9348	^{255}Es	274	1.2295	^{256}Fm	277	1.1194

$$N_{\rm tot} = 9020 \ ; \ \delta_{\rm tot} = 0.8910 \ .$$

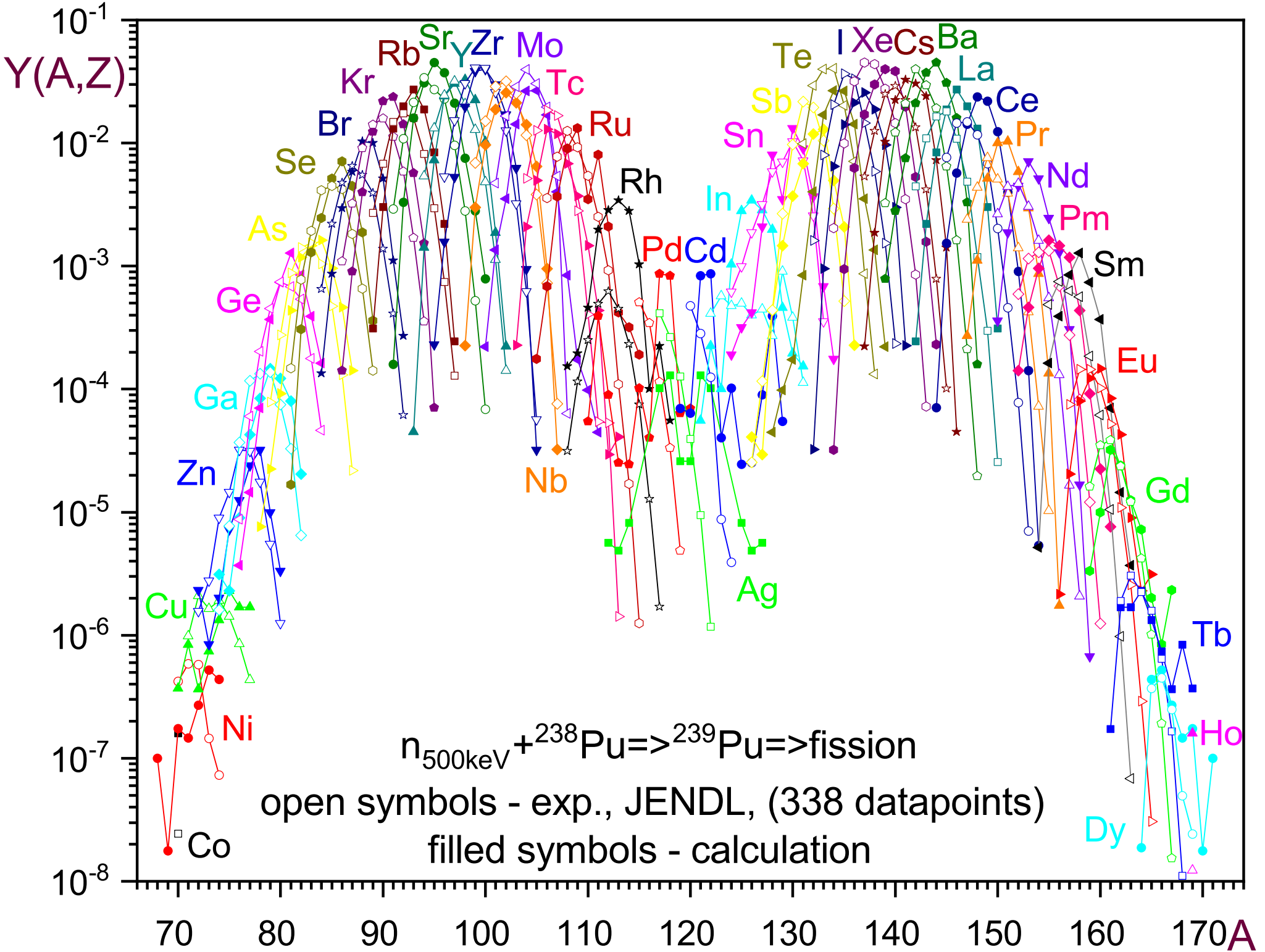
Y(A,Z)
10-1
10-2
10-3
10-4
10-5
10-6
10-7
10-8
70
80
90
100
110
120
130
140
150
160
170
A
Co
Ni
Cu
Zn
Ga
Ge
As
Se
Br
Kr
Rb
Sr
Y
Zr
Mo
Tc
Ru
Rh
Pd
Cd
In
Sn
Sb
Te
I
Xe
Cs
Ba
La
Ce
Pr
Nd
Pm
Sm
Eu
Gd
Tb
Dy
Ho
Ag
Nb
n500keV+238Pu=>239Pu=>fission
open symbols - exp., JENDL, (338 datapoints)
filled symbols - calculation

The deformation energy

The deformation energy of the fragment evaluated relatively to the ground-state deformation β_0 is approximated as

$$E_{\rm def}(\beta) = (C_{\rm ld} + C_{\rm sc})\frac{(\beta - \beta_0)^2}{2},$$

where $C_{\rm ld}$ is the liquid-drop stiffness (quadrupole deformation), $C_{\rm sc} \approx -0.05\, C_{\rm ld}\, \delta_{\rm shell}$ is the shell-correction stiffness.

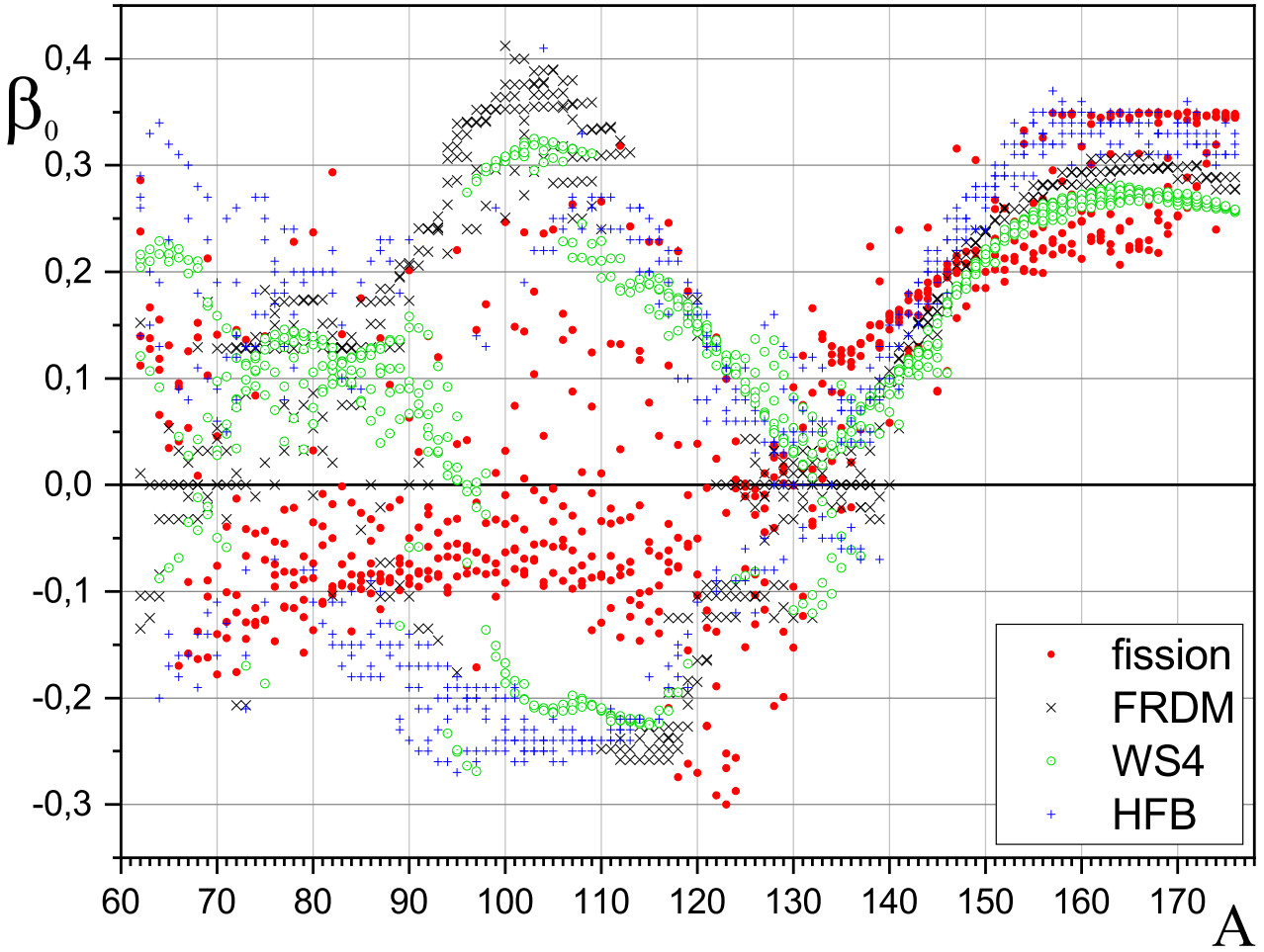

FRDM - P. Moller, et al., At. Data Nucl. Data Tabl. (2016). **WS4** - N. Wang, et al., Phys. Lett. B 734, 215 (2014).

HFB - S. Goriely, et al., Phys. Rev. C 88, 061302 (2013). [The values of β_0 for 634 nuclei to describe 9020 data points.]

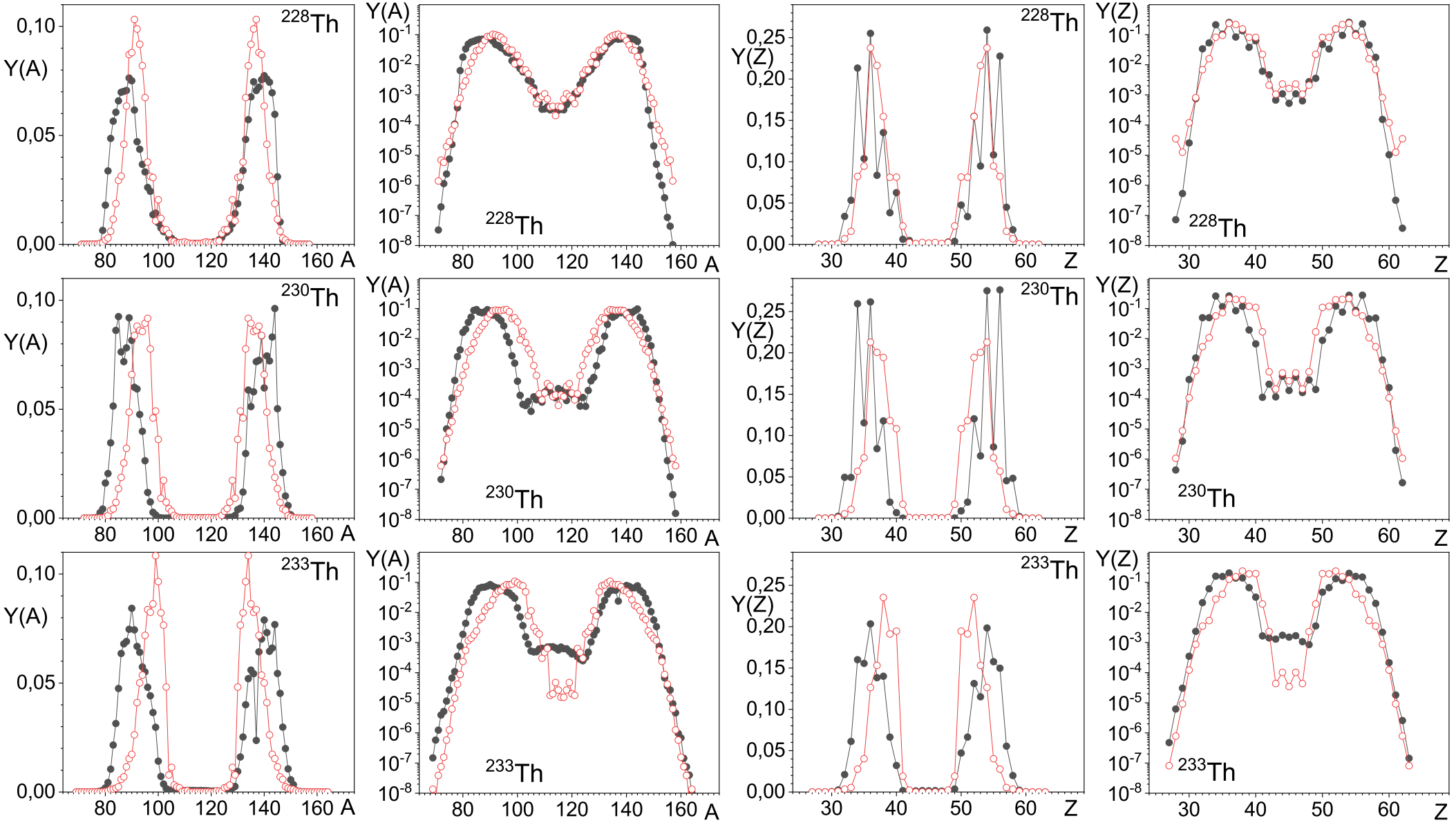

The mass $Y(A)$ and charge $Y(Z)$ distributions distributions of fission fragments for the reactions $n_{th.}+^{227}Th \rightarrow ^{228}Th \rightarrow f$, $n_{th.}+^{229}Th \rightarrow ^{230}Th \rightarrow f$, and $n_{500keV}+^{232}Th \rightarrow ^{233}Th \rightarrow f$ in linear and logarithmic scales calculated in the model (open dots) with the experimental data (filled dots) [JENDL].

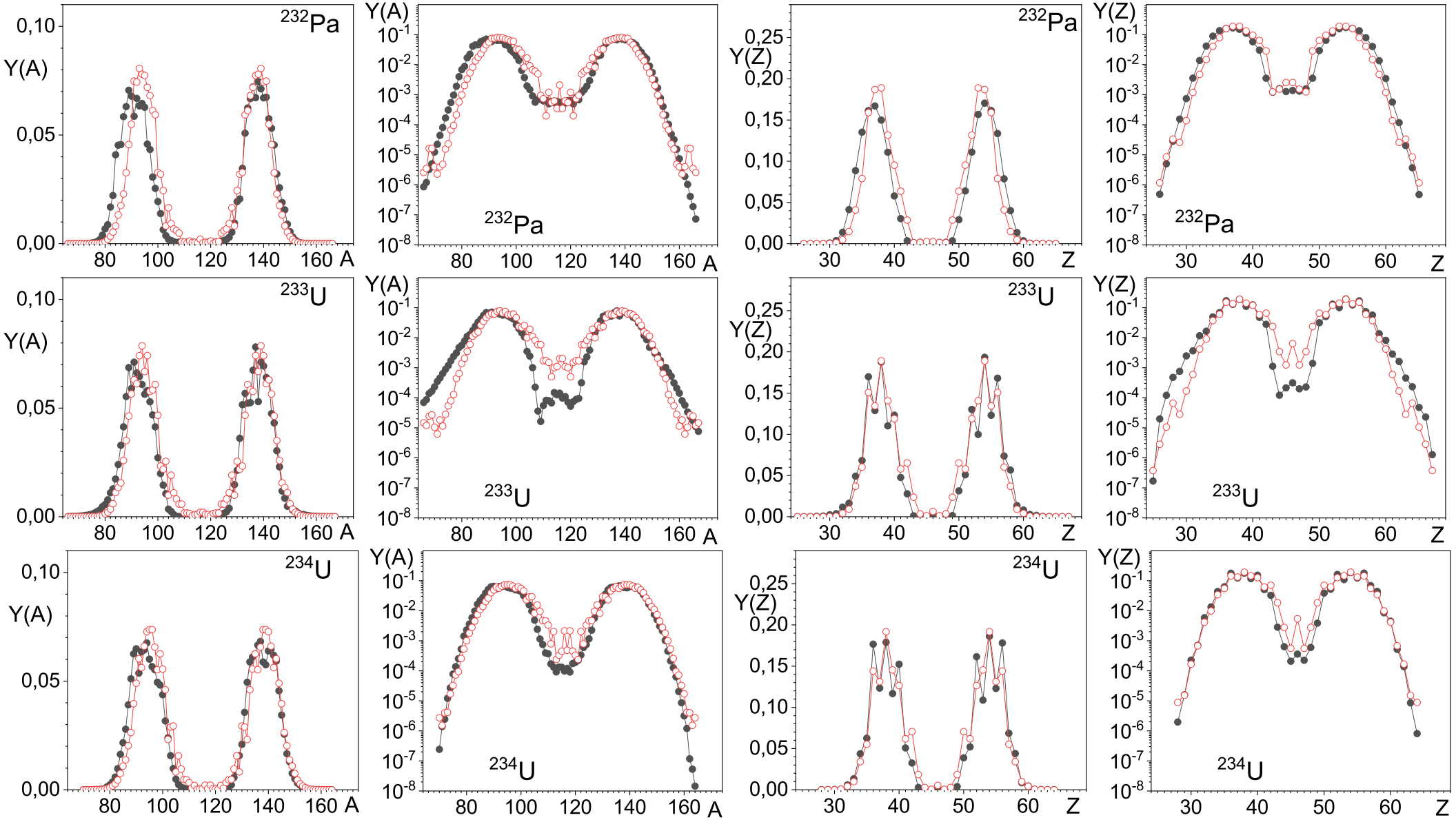

The mass $Y(A)$ and charge $Y(Z)$ distributions distributions of fission fragments for the reactions $n_{500keV}+^{231}Pa\rightarrow^{233}Pa\rightarrow f$, $n_{th.}+^{232}U\rightarrow^{233}U\rightarrow f$, and $n_{th.}+^{233}U\rightarrow^{234}U\rightarrow f$ in linear and logarithmic scales calculated in the model (open dots) with the experimental data (filled dots) [JENDL].

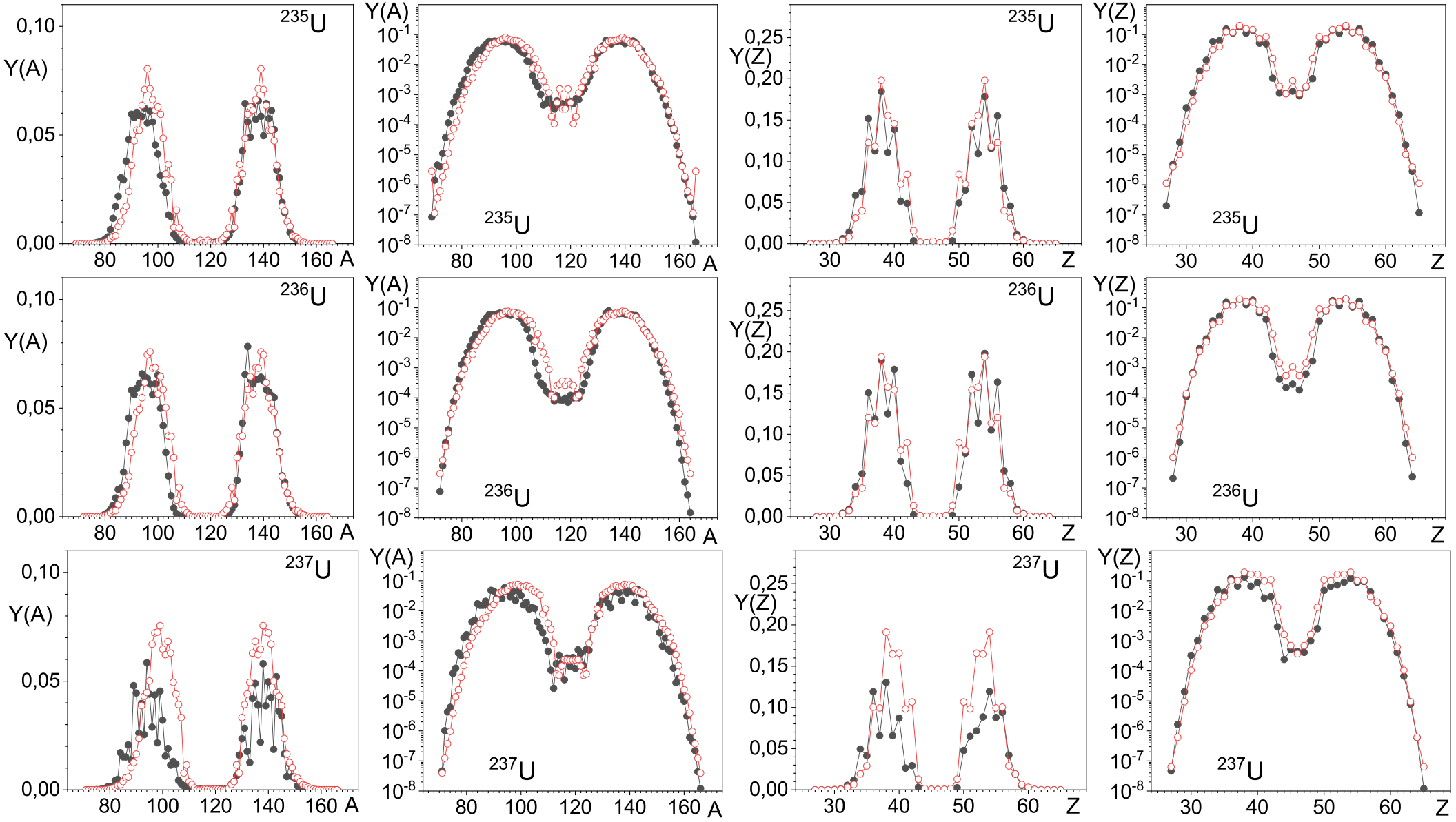

The mass $Y(A)$ and charge $Y(Z)$ distributions distributions of fission fragments for the reactions $n_{500keV}+^{234}U\rightarrow^{235}U\rightarrow f$, $n_{th.}+^{235}U\rightarrow^{236}U\rightarrow f$, and $n_{500keV}+^{236}U\rightarrow^{237}U\rightarrow f$ in linear and logarithmic scales calculated in the model (open dots) with the experimental data (filled dots) [JENDL].

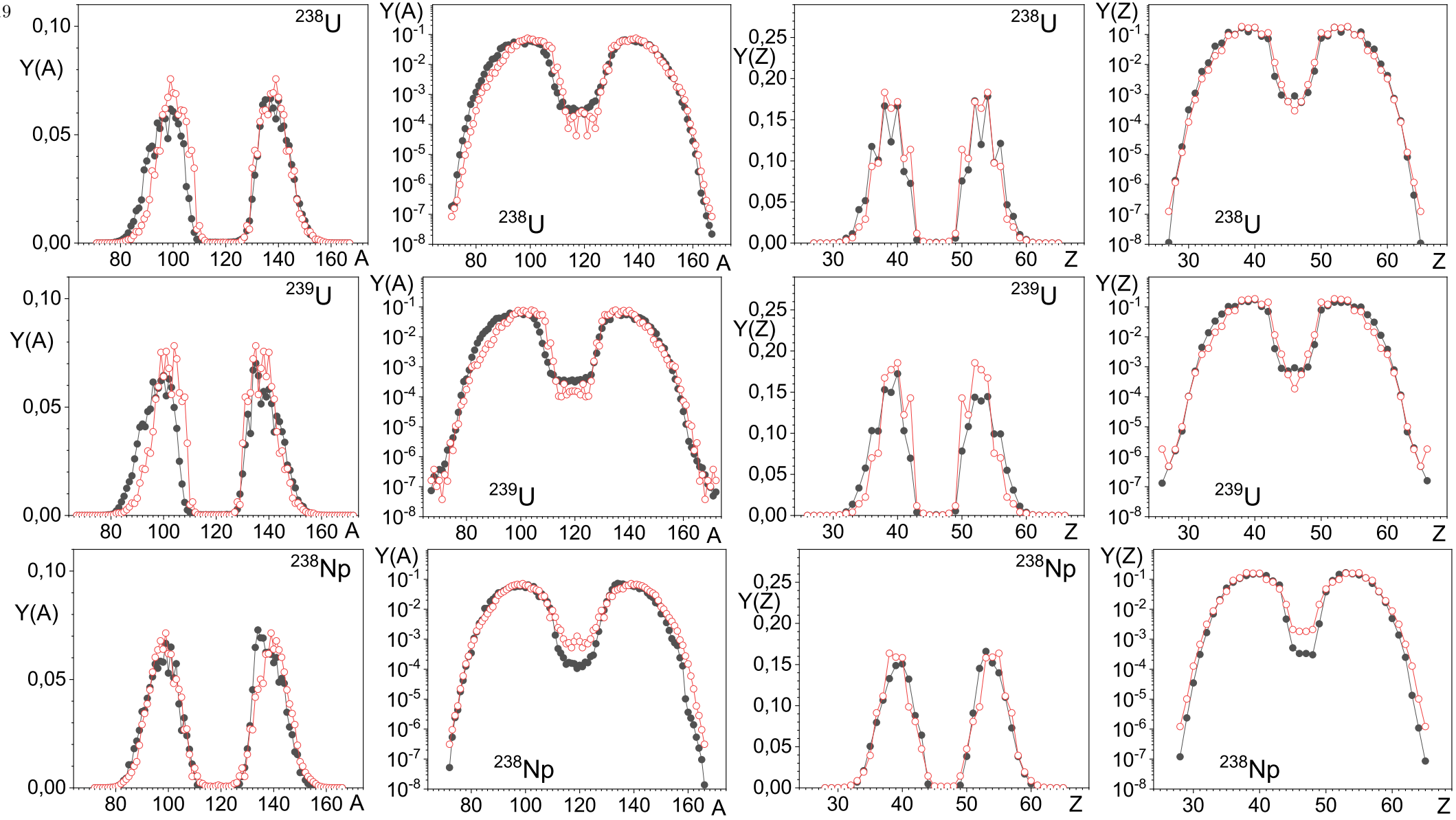

The mass $Y(A)$ and charge $Y(Z)$ distributions distributions of fission fragments for the reactions $n_{500keV}+^{237}U\rightarrow^{238}U\rightarrow f$, $n_{500keV}+^{238}U\rightarrow^{239}U\rightarrow f$, and $n_{th.}+^{237}Np\rightarrow^{238}Np\rightarrow f$ in linear and logarithmic scales calculated in the model (open dots) with the experimental data (filled dots) [JENDL].

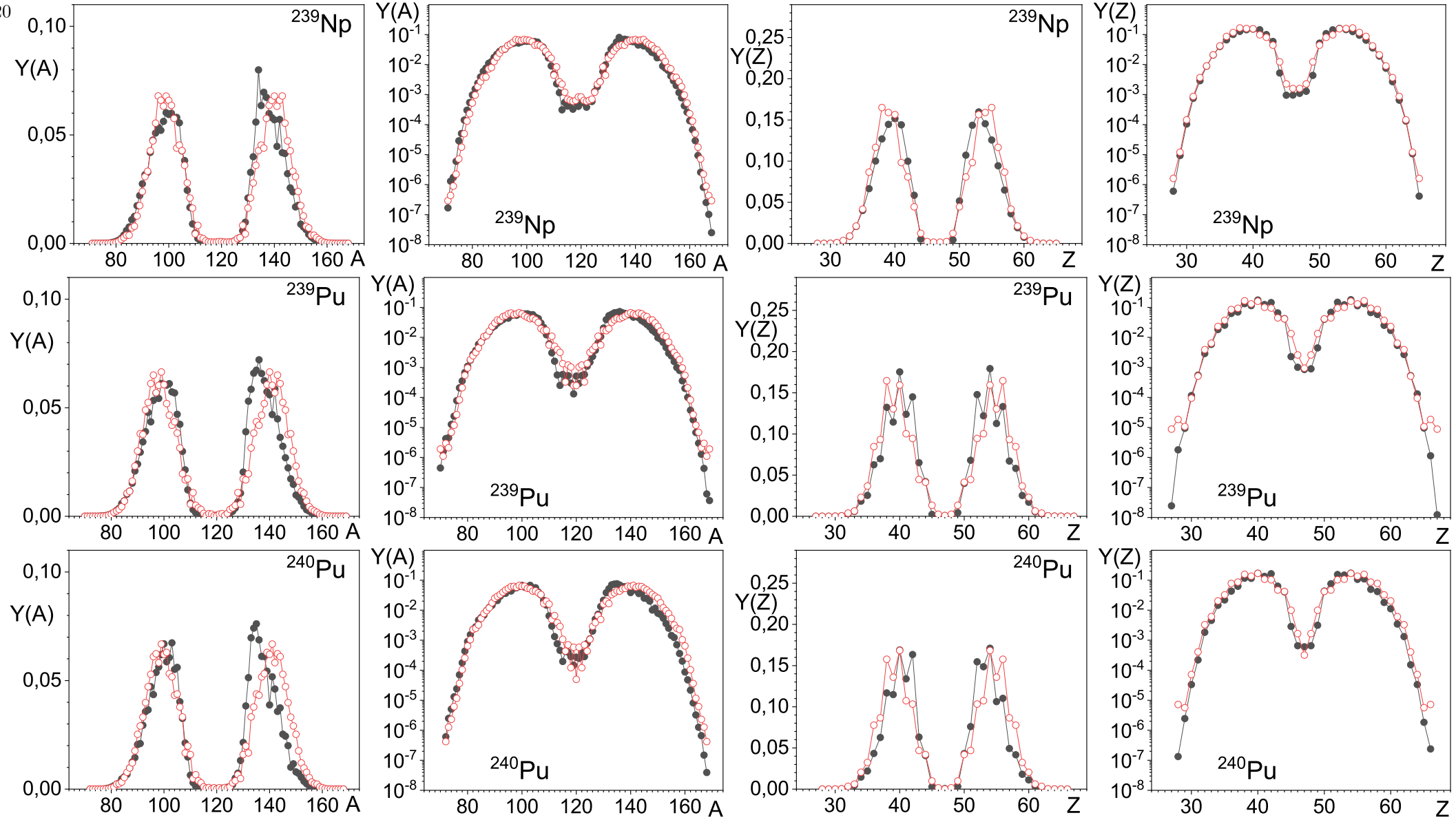

The mass $Y(A)$ and charge $Y(Z)$ distributions distributions of fission fragments for the reactions $n_{500keV}+^{238}Np \rightarrow ^{239}Np \rightarrow f$, $n_{500keV}+^{238}Pu \rightarrow ^{239}Pu \rightarrow f$, and $n_{th.}+^{239}Pu \rightarrow ^{240}Pu \rightarrow f$ in linear and logarithmic scales calculated in the model (open dots) with the experimental data (filled dots) [JENDL].

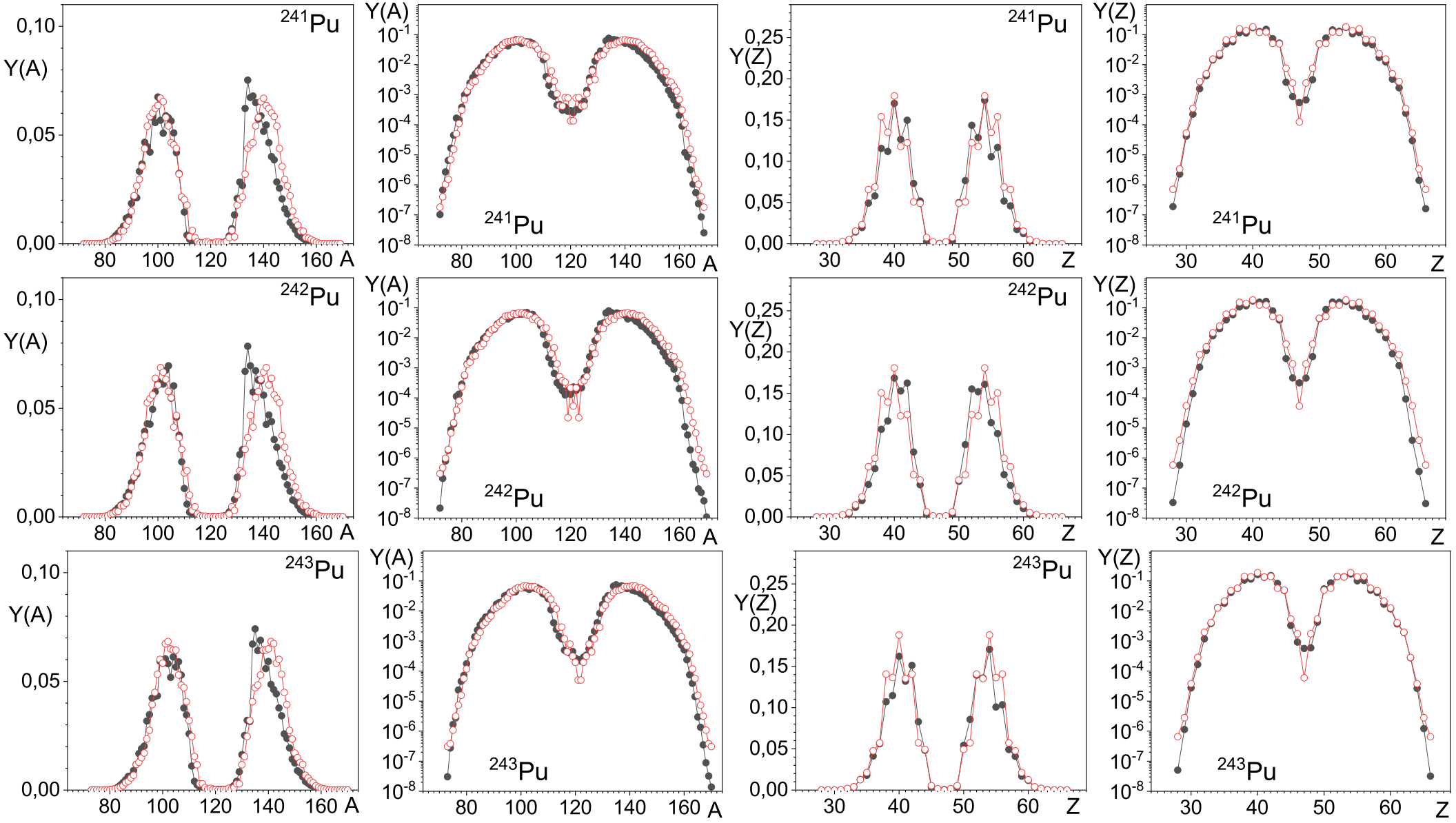

The mass $Y(A)$ and charge $Y(Z)$ distributions distributions of fission fragments for the reactions

$$n_{th.}+^{240}Pu\rightarrow^{241}Pu\rightarrow f,\ n_{th.}+^{241}Pu\rightarrow^{242}Pu\rightarrow f,\ n_{th.}+^{242}Pu\rightarrow^{243}Pu\rightarrow f$$

in linear and logarithmic scales calculated in the model (open dots) with the experimental data (filled dots) [JENDL].

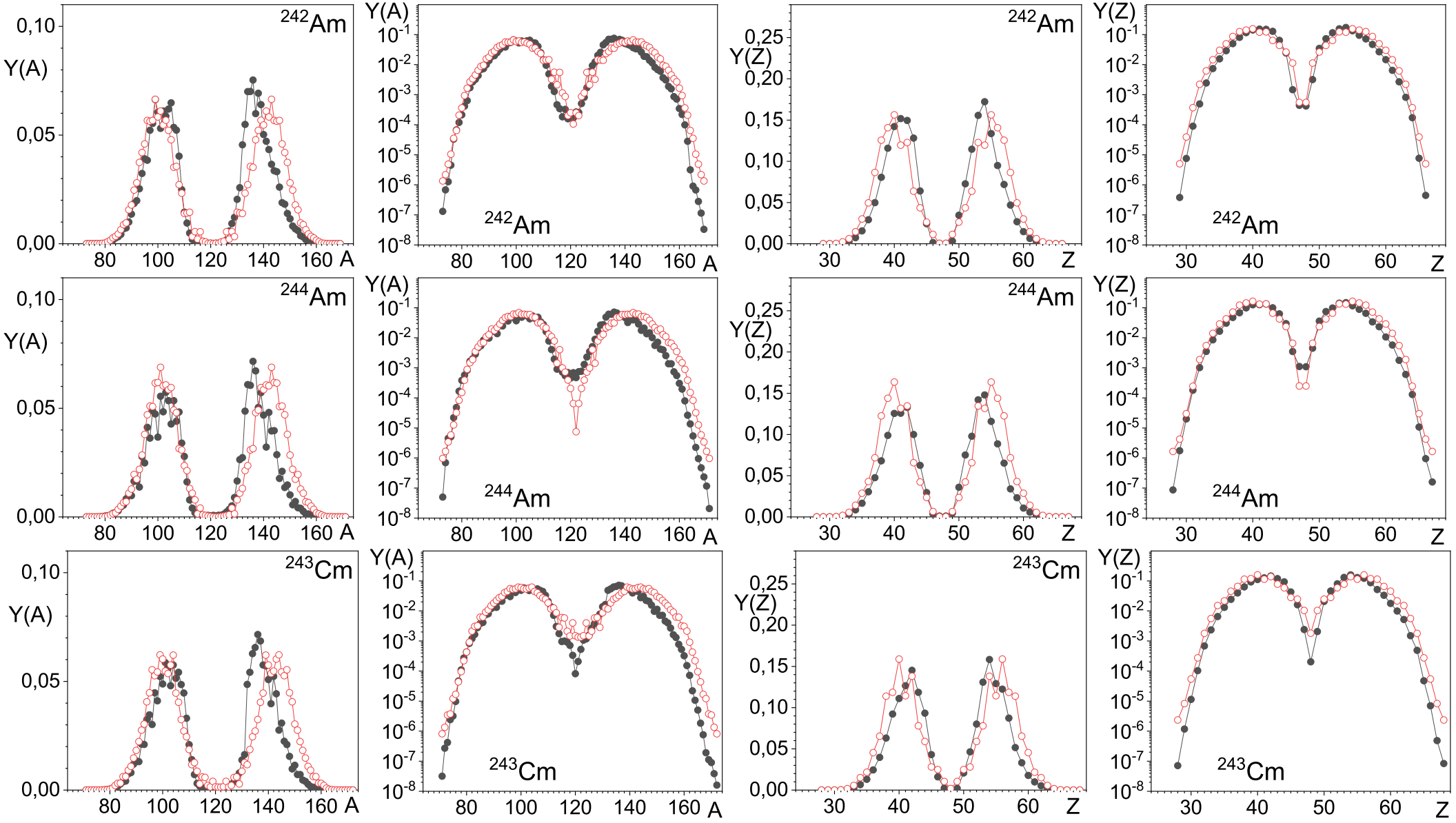

The mass $Y(A)$ and charge $Y(Z)$ distributions distributions of fission fragments for the reactions $n_{th.}+^{241}Am \rightarrow ^{242}Am \rightarrow f$, $n_{500keV}+^{243}Am \rightarrow ^{244}Am \rightarrow f$, and $n_{500keV}+^{242}Cm \rightarrow ^{243}Cm \rightarrow f$ in linear and logarithmic scales calculated in the model (open dots) with the experimental data (filled dots) [JENDL].

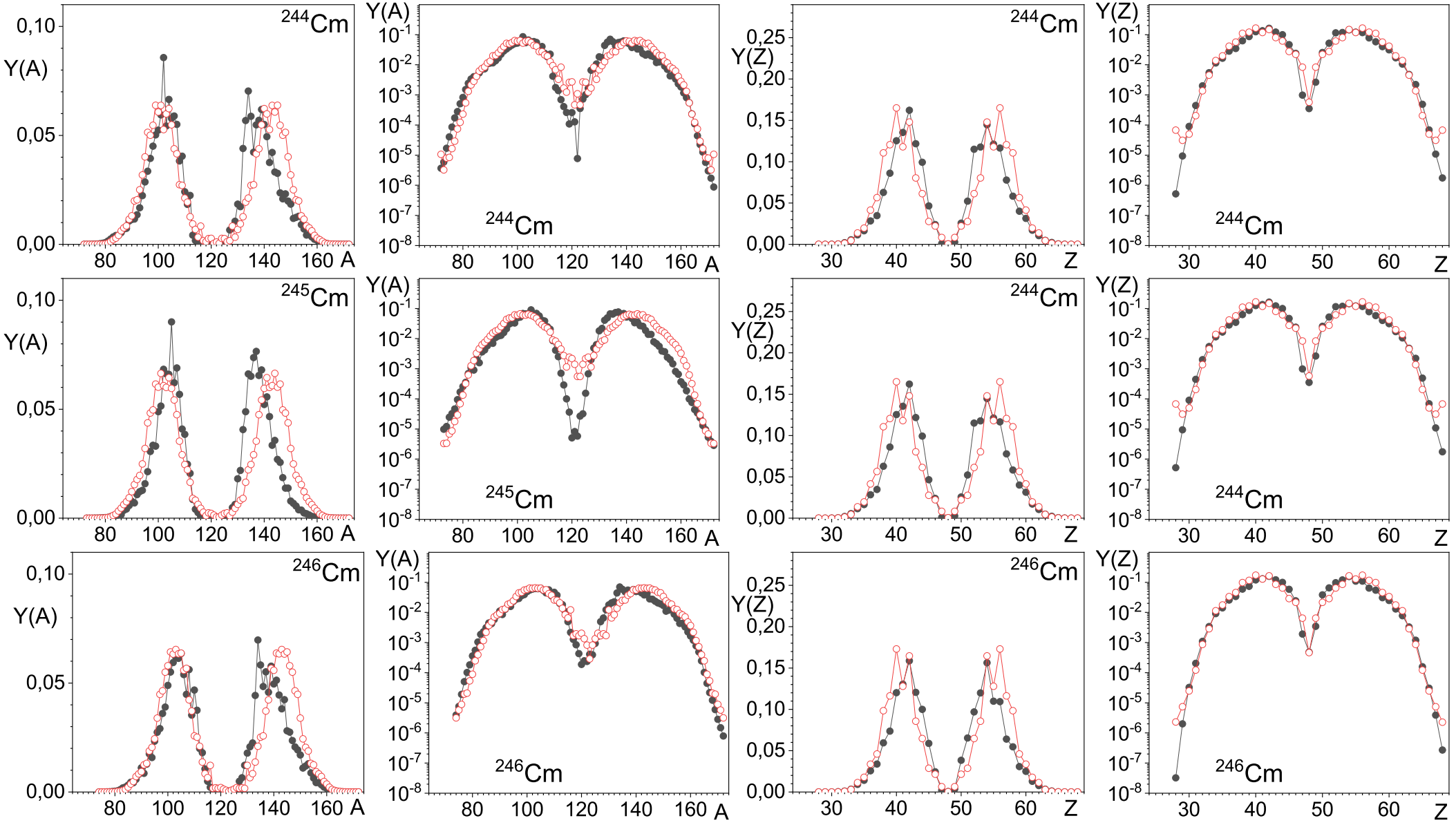

The mass $Y(A)$ and charge $Y(Z)$ distributions distributions of fission fragments for the reactions $n_{th.}+^{243}Cm \rightarrow ^{244}Cm \rightarrow f$, $n_{500keV}+^{244}Cm \rightarrow ^{245}Cm \rightarrow f$, and $n_{th.}+^{245}Cm \rightarrow ^{246}Cm \rightarrow f$ in linear and logarithmic scales calculated in the model (open dots) with the experimental data (filled dots) [JENDL].

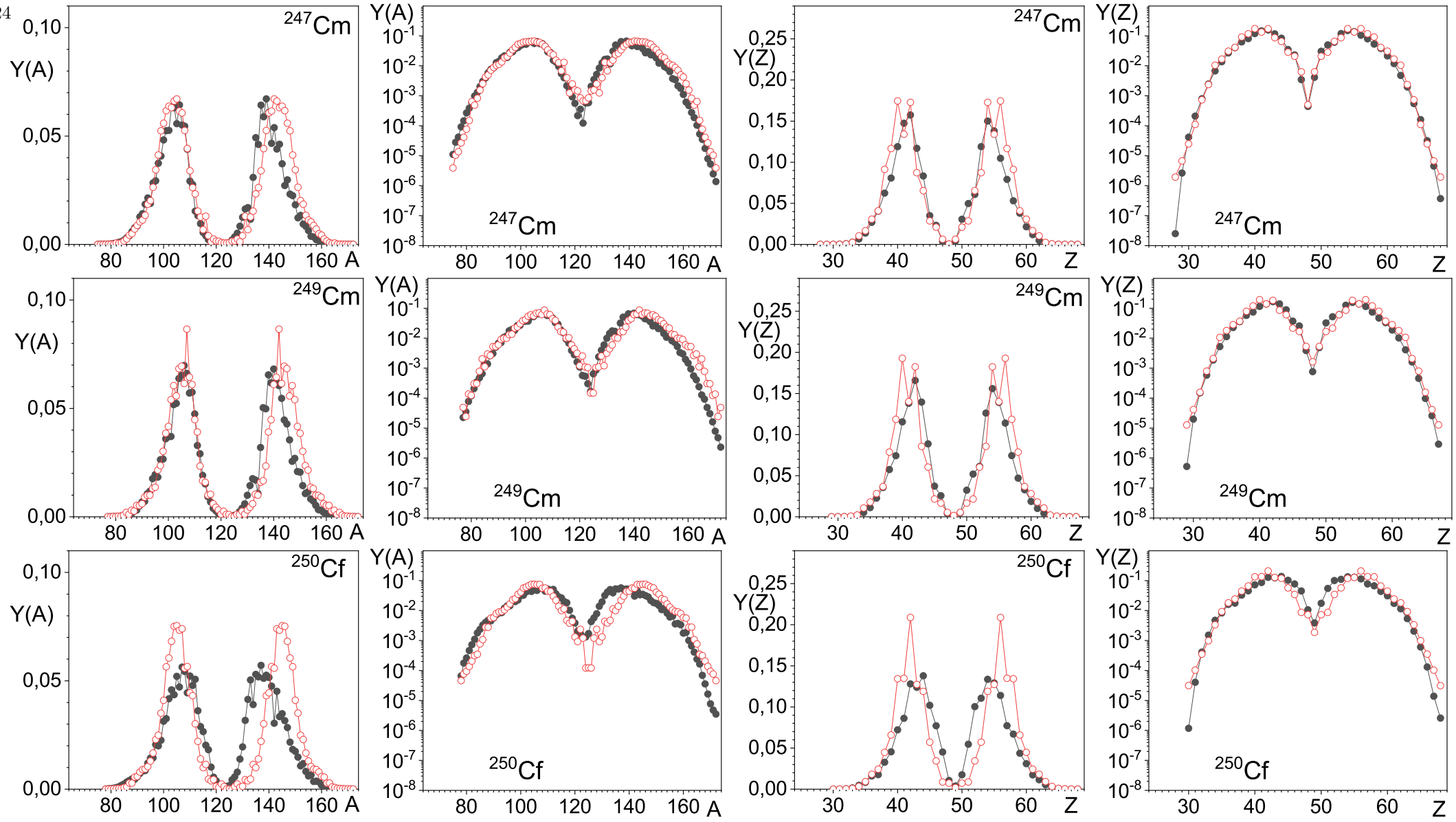

The mass $Y(A)$ and charge $Y(Z)$ distributions distributions of fission fragments for the reactions $n_{500keV}+^{246}Cm\rightarrow^{247}Cm\rightarrow f$, $n_{500keV}+^{248}Cm\rightarrow^{249}Cm\rightarrow f$, and $n_{th.}+^{249}Cf\rightarrow^{250}Cf\rightarrow f$ in linear and logarithmic scales calculated in the model (open dots) with the experimental data (filled dots) [JENDL].

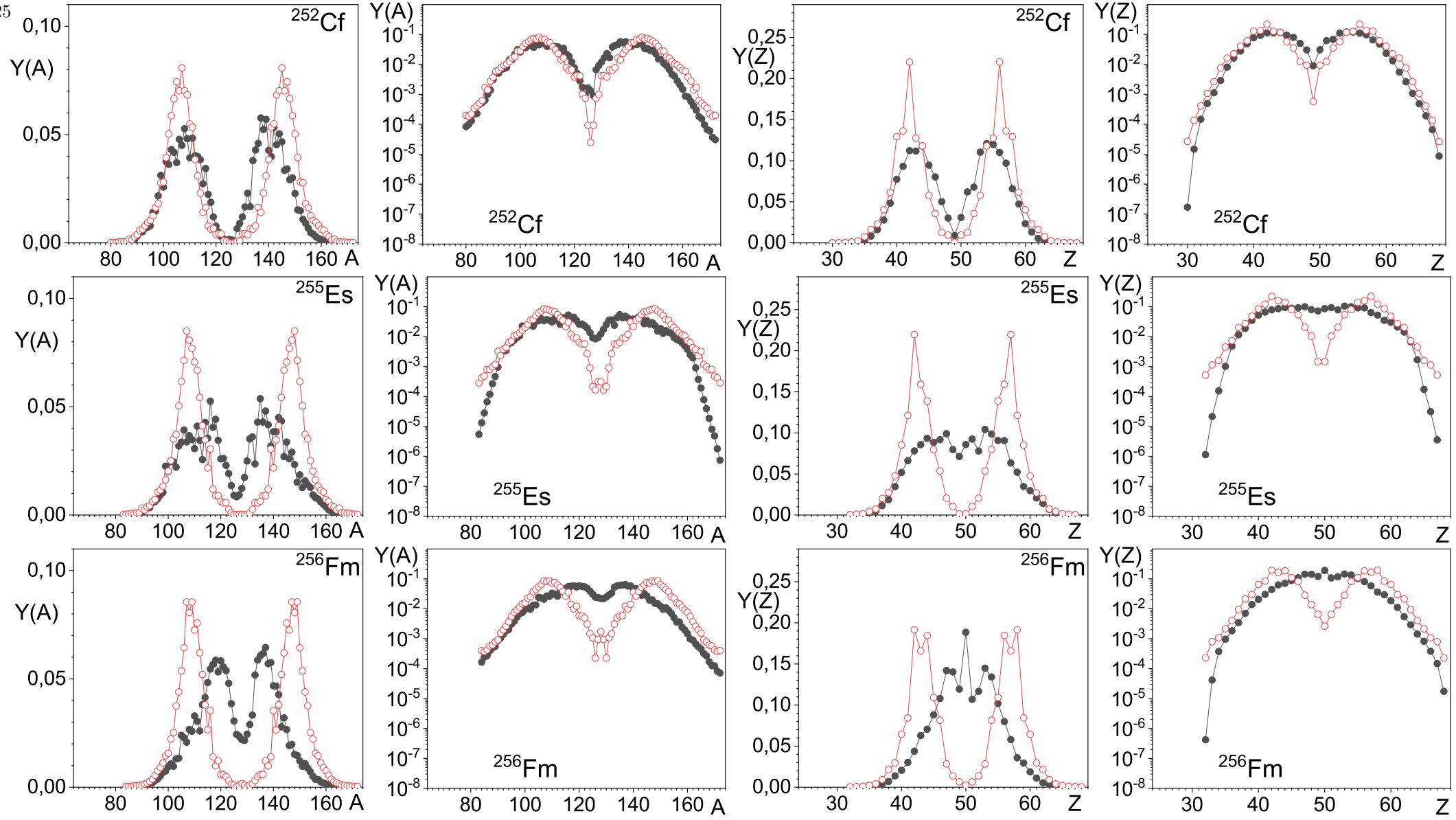

The mass $Y(A)$ and charge $Y(Z)$ distributions distributions of fission fragments for the reactions $n_{th.}+^{251}Cf \rightarrow ^{252}Cf \rightarrow f$, $n_{th.}+^{254}Es \rightarrow ^{255}Es \rightarrow f$, and $n_{th.}+^{255}Fm \rightarrow ^{255}Fm \rightarrow f$ in linear and logarithmic scales calculated in the model (open dots) with the experimental data (filled dots) [JENDL].

The kinetic energies of the fragments on the infinite distance in the mass centers formed by passing the saddle points 1 and 2 are, respectively,

$$E_{\rm kin}^{s1} = V_{12}^{\rm Coulomb\ s1}(r_{1\alpha}^{s1} + r_{2\alpha}^{s1}, \beta_1^{s1}, \beta_2^{s1}) + V_{12}^{\rm nucl\ s1}(r_{1\alpha}^{s1} + r_{2\alpha}^{s1}, \beta_1^{s1}, \beta_2^{s1}) + V_{2\alpha}^{s1}(r_{2\alpha}^{s1}, \beta_2^{s1}),$$
$$E_{\rm kin}^{s2} = V_{12}^{\rm Coulomb\ s2}(r_{1\alpha}^{s2} + r_{2\alpha}^{s2}, \beta_1^{s2}, \beta_2^{s2}) + V_{12}^{\rm nucl\ s2}(r_{1\alpha}^{s2} + r_{2\alpha}^{s2}, \beta_1^{s2}, \beta_2^{s2}) + V_{1\alpha}^{s2}(r_{1\alpha}^{s2}, \beta_1^{s2}).$$

The average total kinetic energy ($\overline{TKE}$) is

$$\overline{TKE} = \frac{1}{N_3} \sum_{A_1,Z_1} \int d\beta_1 \int d\beta_2 \left[\rho_{A_1-4}(E_1^{s1})\rho_{A_2}(E_2^{s1})E_{\rm kin}^{s1} + \rho_{A_1}(E_1^{s2})\rho_{A_2-4}(E_2^{s2})E_{\rm kin}^{s2}\right].$$

The experimental and theoretical values of $\overline{TKE}$ of primary fragments (in MeV).

Nucl.	$\overline{TKE}_{\rm teor.}$	$\overline{TKE}_{\rm exp.}$	Nucl.	$\overline{TKE}_{\rm teor.}$	$\overline{TKE}_{\rm exp.}$	Nucl.	$\overline{TKE}_{\rm teor.}$	$\overline{TKE}_{\rm exp.}$
^{228}Th	168.2	-	^{230}Th	167.9	163.6±0.5	^{233}Th	167.8	162
^{232}Pa	170.3	166.6±0.5	^{233}U	173.2	170.7±0.5	^{234}U	173.0	171.5±0.2
^{235}U	173.0	170.58±0.05	^{236}U	172.8	170.6±0.6	^{237}U	172.8	170.5
^{238}U	172.5	-	^{239}U	172.7	170.2±1.4	^{238}Np	175.2	174.7±0.6
^{239}Np	174.8	-	^{239}Pu	177.8	179.7±0.5	^{240}Pu	177.7	178.8±0.5
^{241}Pu	177.8	178.2±0.5	^{242}Pu	177.5	179.00±0.06	^{243}Pu	177.6	179.32±1.8
^{242}Am	180.4	181.6±0.4	^{244}Am	179.9	-	^{243}Cm	183.2	-
^{244}Cm	183.1	-	^{245}Cm	183.0	-	^{246}Cm	182.8	188.5±3.0
^{247}Cm	182.7	-	^{249}Cm	182.1	-	^{250}Cf	188.3	187.3±1.5
^{252}Cf	188.1	-	^{255}Es	190.6	-	^{256}Fm	193.6	-

Four-body system: [The scission is between α-particles.]

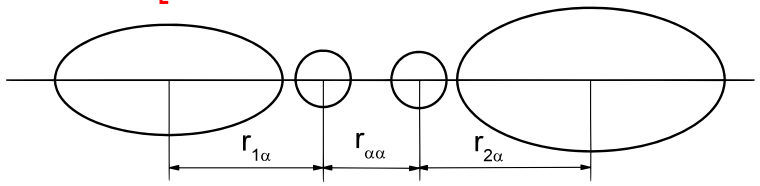

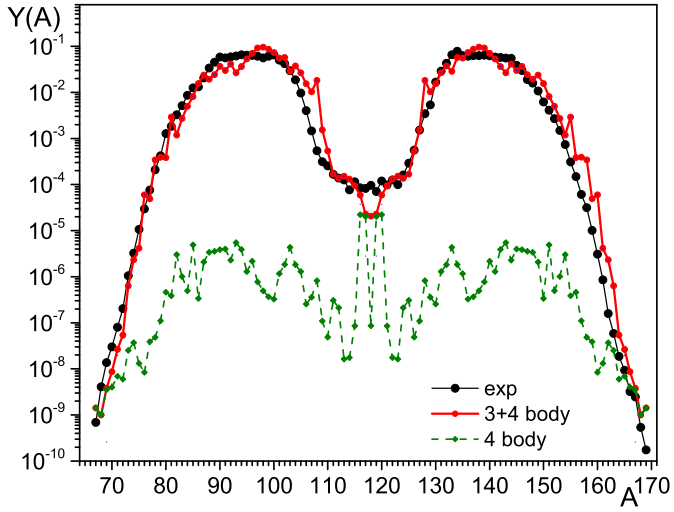

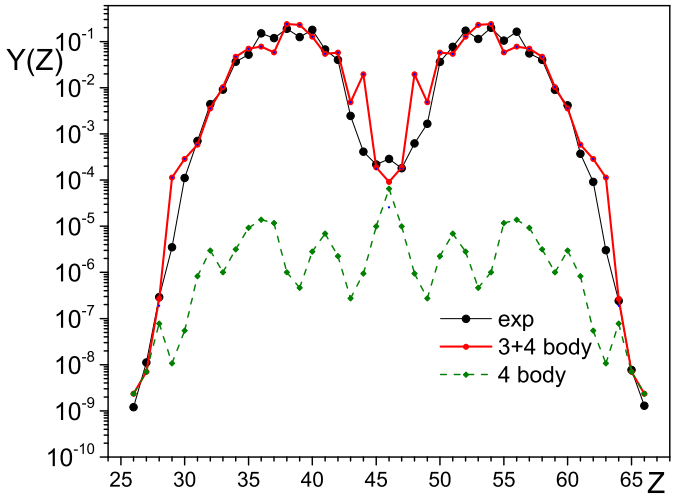

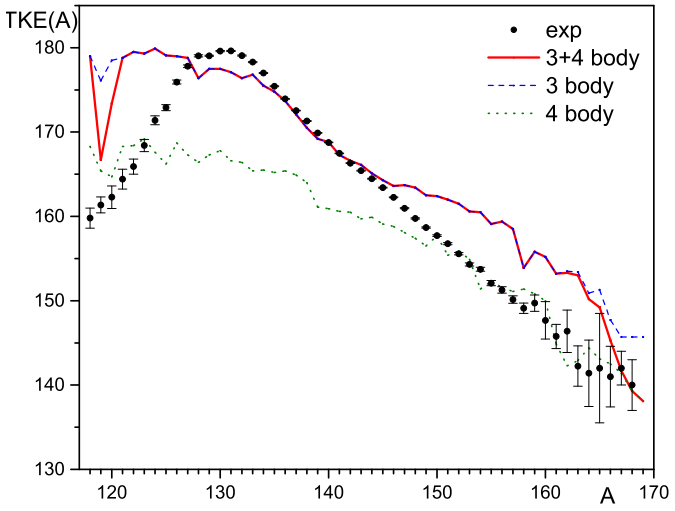

$Y(A)$, $Y(Z)$, and $TKE(A)$ for the reaction $n_{th}+^{235}U$. The experimental data: $Y(A)$ and $Y(Z)$ $\Rightarrow$ JENDL; TKE(A) $\Rightarrow$ Sh. Zeynalov, et al., ISINN-13, 351 (2006).

Four-body system: [The scission is between α-particles.]

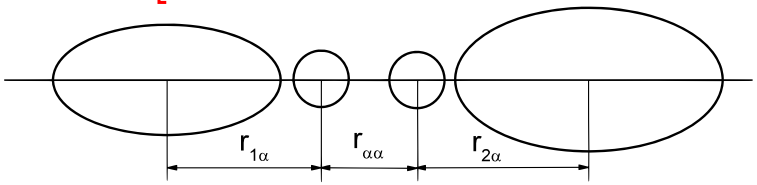

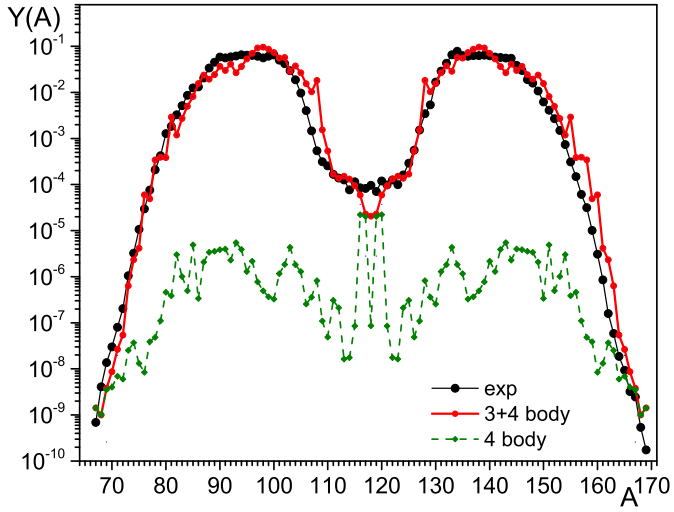

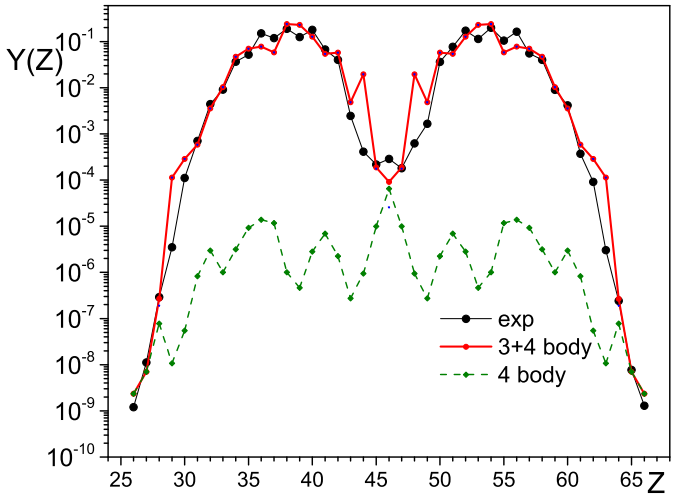

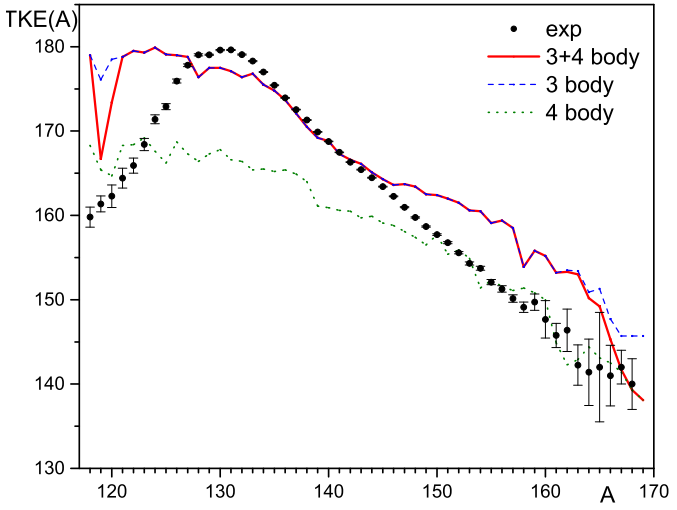

$Y(A)$, $Y(Z)$, and $TKE(A)$ for the reaction $n_{th}+^{235}U$. The experimental data: $Y(A)$ and $Y(Z)$ $\Rightarrow$ JENDL; TKE(A) $\Rightarrow$ Sh. Zeynalov, et al., ISINN-13, 351 (2006).

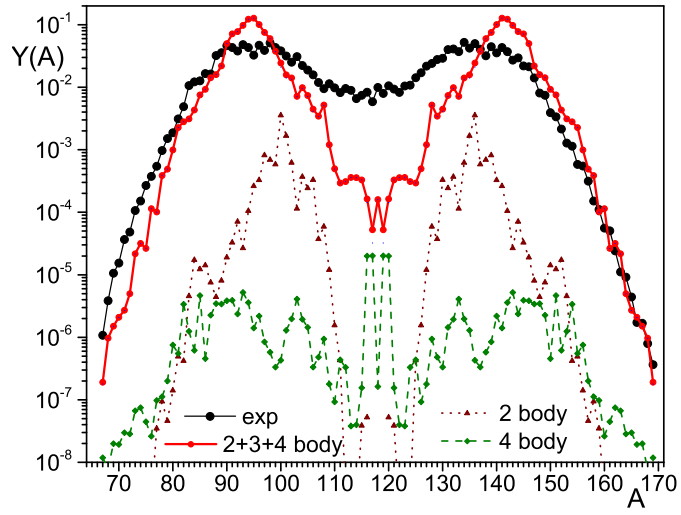

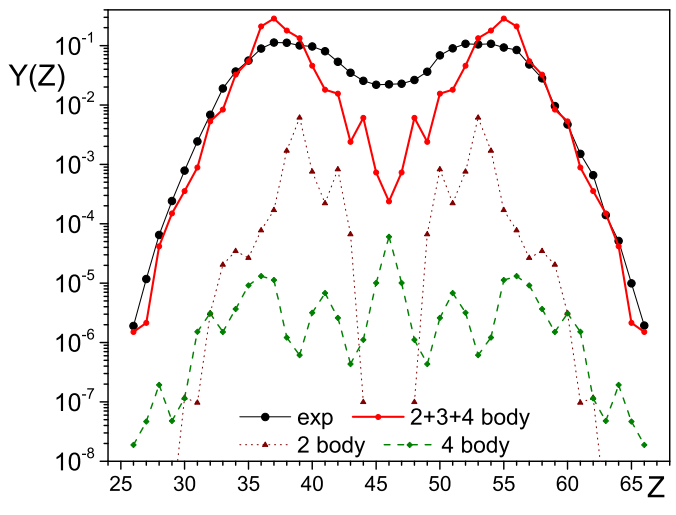

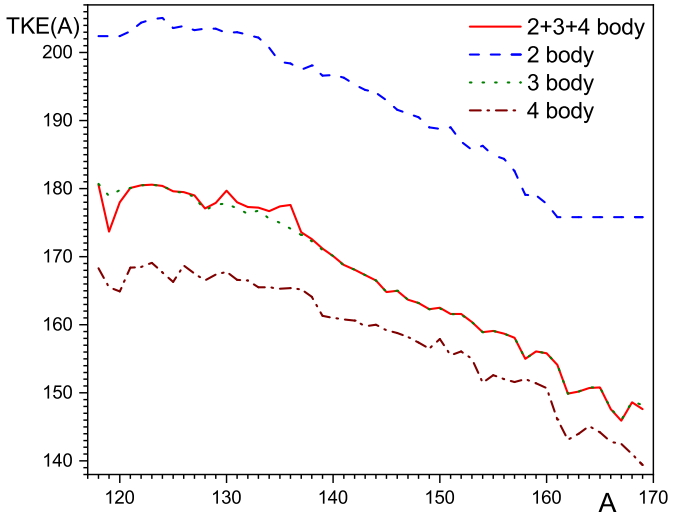

$Y(A)$, $Y(Z)$, and $TKE(A)$ for the reaction $n_{14MeV}+^{235}U$. The experimental data: $Y(A)$ and $Y(Z)$ $\Rightarrow$ JENDL.

CONCLUSIONS

1. The model for the description of the binary fission based on the three-body scission configuration is proposed. The three-body scission configuration consists of two heavy fragments and α-particle located between them. Such presentation of scission configuration gives the possibility to describe the processes occurring in the neck during the fission of the nucleus.

2. There are the saddle points between touching and well-separated heavy deformed fragments of the three-body system. After passing through the saddle point during fission the α-particle is fused with the nearest nucleus.

3. The yield of the fission fragments $Y(A,Z)$ is proportional to the number of levels at the saddle points.

4. The values of the ground-state deformation parameters of heavy fragments are defined in the description of the nuclide yields.

5. There are the two-, three-, and four-body fission modes.

6. The yields of nuclides $Y(A,Z)$, the mass $Y(A)$ and charge $Y(Z)$ fission fragment distributions, as well as, the average total kinetic energy $\overline{TKE}$ of the fragments are well described simultaneously in the model.

Thank you very much for your attention!

The talk is based on the papers:

- *V. Yu. Denisov, I. Yu. Sedykh, Eur. Phys. J. A 57, 129 (2021).*
- *V. Yu. Denisov, Eur. Phys. J. A 58, 188 (2022).*